ACS Sustainable Chemistry & Engineering

pubs.acs.org/journal/ascecg

Research Article

Cationic Lignin as an Efficient and Biorenewable Antimicrobial Material

Karen Acurio Cerda, Mark Kathol, Gunjan Purohit, Ehsan Zamani, Martha D. Morton, Oleh Khalimonchuk, Rajib Saha, and Shudipto Konika Dishari*

Cite This: *ACS Sustainable Chem. Eng.* 2023, 11, 10364−10379

Read Online

ACCESS | Metrics & More | Article Recommendations | Supporting Information

ABSTRACT: In this work, we utilized an inexpensive and naturally abundant polymer lignin and functionalized it with quaternary ammonium groups to yield a cationic antimicrobial, QAL. As opposed to non-cationic alkali lignin (AL), a relatively low concentration of cationic QAL (∼25−150 μg/mL) exerted strong bacteriostatic and bacteriolytic effects against both wild-type and kanamycin (kan)-resistant *E. coli* (∼90% dead cells, ∼90−100% growth inhibition with a 1 h treatment). Treatment with 25 μg/mL QAL exposed lipid (Nile red staining) and roughened the bacterial cell envelope (from ∼4.9 to 12.9 nm). Inner membrane damage was also evident as an increased amount of leakage of the cytoplasmic enzyme was evidenced by the increase in treatment time and QAL concentration. Additionally, a Langmuir-like monolayer coverage of QAL onto bacteria was identified, which agreed with zeta potential measurements and suggested electrostatic binding as the major mechanism of antimicrobial action of QAL. Lastly, QAL showed no/minimal cytotoxicity against human embryonic kidney cells (90−100% cell viability) within the concentration range (0−300 μg/mL) in which QAL killed and completely inhibited the growth of bacteria. The development of such efficient, biorenewable antimicrobial materials from lignin can pave the way for effectively addressing antibiotic resistance and enabling biomass valorization simultaneously.

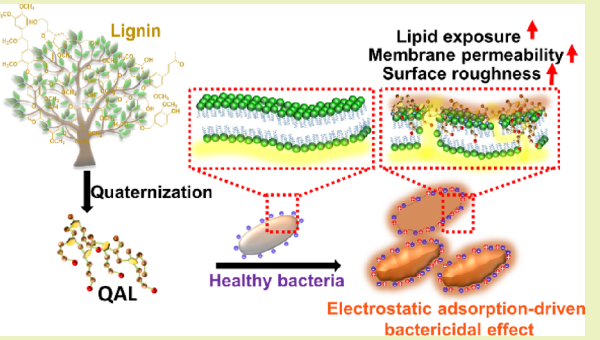

KEYWORDS: *lignin, polymer, biomass valorization, bacteria, antimicrobial, antibiotic-resistant, sustainable, biorenewable*

INTRODUCTION

Antibiotic resistance, a serious public health concern, can be responsible for the death of ∼10 million people per year by 2050.[1] The overuse/misuse of antibiotics is one of the major reasons for drug-resistant infections.[2−4] On the other hand, a large fraction of hospital-acquired, resistant bacterial infections originate from touch surfaces, healthcare equipment, implants, catheters, and so on. Moreover, the wastewater coming from hospitals and localities frequently contains antibiotic-resistant bacteria[5,6] requiring effective antimicrobial coatings and disinfecting solutions.

Over the years, a broad range of metal-based,[7−9] synthetic,[10−23] and bio-based[24−31] antimicrobial agents have been reported to demonstrate bacteriostatic or bacteriolytic activities. Of these, the non-specific binding-induced antimicrobial processes stand unique as even the notorious bacterial strains (ESKAPE pathogens) often find it difficult to develop resistance against these processes.[32,33] The electrostatic binding with negative charges of lipopolysaccharides of the bacterial cell envelope[32,34] and the bacteriostatic/bacteriolytic action mechanism of this unique class of antimicrobials are facilitated by their cationic functionalities. This also enables us to bypass some of the specific targeting modes (e.g., inhibition of protein synthesis) to which bacteria, like kanamycin-resistant *E. coli*, show resistance typically. The cationic antimicrobials that have risen to prominence so far are the following (Table S1): antimicrobial peptides (AMPs),[14,35−37] π-conjugated oligo-/polyelectrolytes (CCOEs/CCPEs),[1,13,19,22,32,38,39] and their composites with organic/inorganic nanoparticles.[40−43] Typically, the length and functionalities of the backbones and side chains of these cationic antimicrobials determine whether the antimicrobial molecules will coat or intercalate within the bacterial cell envelope. The electrostatic binding is followed by physical, mechanical, and morphological alterations[11,20,44−52] of the bacterial cell envelope as well as alteration of bacterial omics,[11,53−55] arresting further growth of bacteria or causing cell death. While many of these synthetic antimicrobials hold promise, the use and disposal of these may cause environ-

Received: March 9, 2023
Revised: June 15, 2023
Published: July 3, 2023

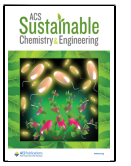

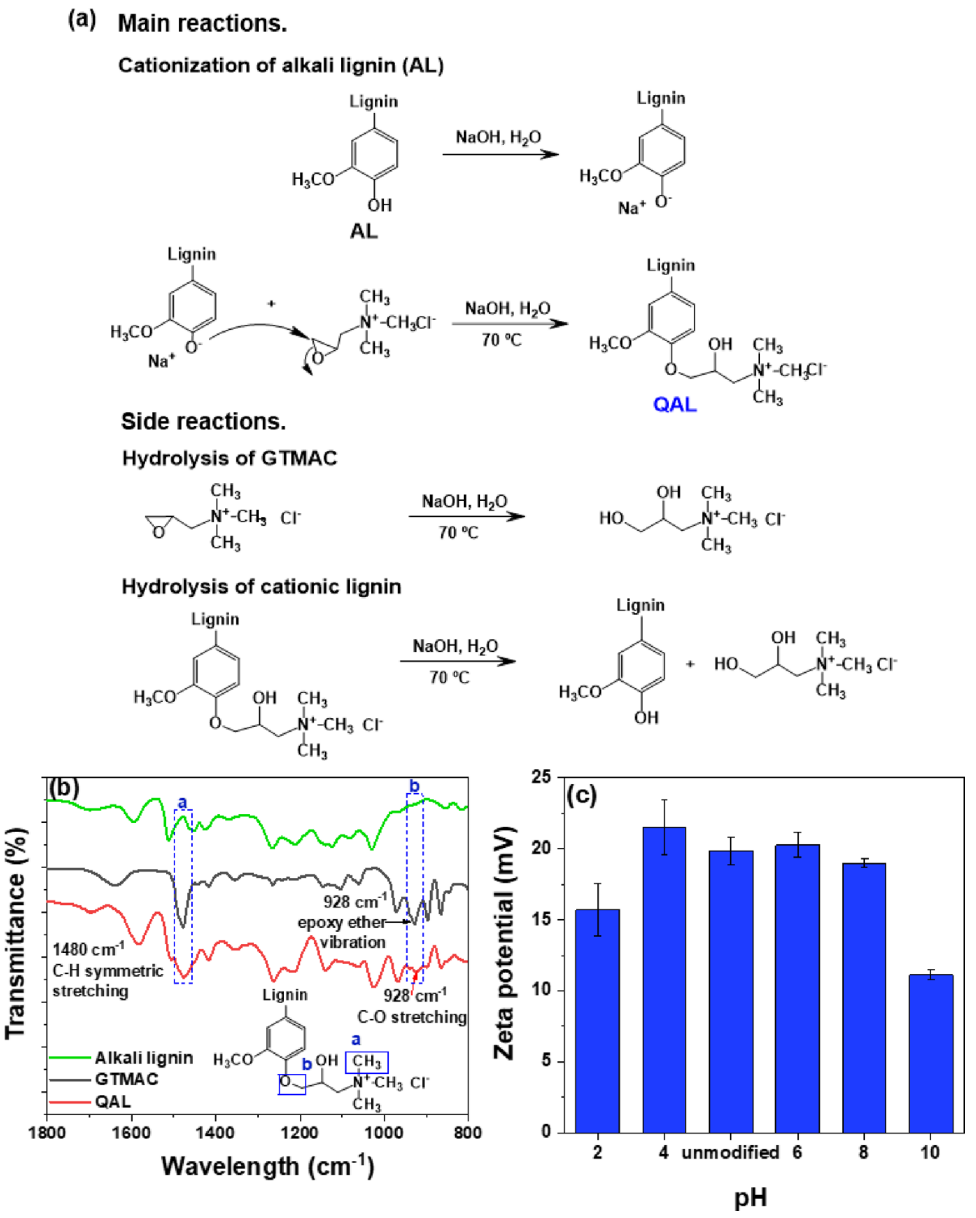

Figure 1. (a) Synthetic scheme with reaction mechanism of AL and GTMAC under basic conditions. (b) FT-IR spectra of AL, GTMAC, and QAL. (c) Zeta potential of QAL at different pHs. The error bars were calculated based on the standard deviations.

mental concerns.[56] Also, the Centers for Disease Control and Prevention (CDC) estimated the expense of handling antibiotic resistance as ~$55 billion/year in the U.S.[57] Therefore, if low-cost, high-efficacy, cationic antimicrobials can be developed from green and eco-friendly materials, we will not only be able to fight against antibiotic-resistant bacteria effectively and economically but will also be able to save human, animal, and aquatic life.

Here, we report an effective cationic antimicrobial derived from a green, inexpensive precursor, lignin. Lignin is the second most naturally abundant polymer[58] and a major constituent of plant cell walls.[59] Lignin is not only a major component of agricultural wastes but also a byproduct of pulp and paper mills[59,60] and biorefineries.[60,61] Every year, ~100 million tons of lignin is produced worldwide.[62] Nonetheless, only a small fraction of this lignin is valorized, and the rest is simply burnt or discarded.[59,62] In addition to many attractive properties,[63−68] the antimicrobial properties of neutral lignin and lignin-based nanoparticles have been explored recently (Table S1).[29,31,69−71] Primarily, the antimicrobial property of lignin is attributed to its methyl and phenolic hydroxyl (-OH) groups.[29] However, the neutral lignin is insoluble in water at neutral pH and thus requires an alkaline environment[72] or organic solvents (DMSO)[70] to study its antimicrobial properties. Moreover, a very high concentration of these neutral lignin-based antimicrobials was required to achieve 100% growth inhibition of bacteria (minimum inhibitory concentration (MIC) of ~0.5−12 mg/mL,[70,71] %CFU reduction of ~30% with 10 mg/mL).[29] Other works used lignin as a carrier of antimicrobial metal (Ag) nanoparticles[29,73,74] or as a support to grow metal salt nanocrystals.[43] However, in such cases, metals were presented as the main active agents, and the individual contribution of neutral/cationic lignin as an antimicrobial in these composites remains to be elucidated.[29,74] Acid-treated[75] or cationized lignins[30,76−78] have shown promise (Table S1), but their

https://doi.org/10.1021/acssuschemeng.3c01414
ACS Sustainable Chem. Eng. 2023, 11, 10364−10379

antimicrobial properties are partially comprehended. With limited efforts and varying strategies to measure antimicrobial properties (inhibition zone diameter *vs.* MIC *vs.* % colony forming unit (CFU) reduction) from one report to another, comparing their efficacies is cumbersome. Most importantly, a rigorous and systematic effort to unravel the bacteriostatic/bacteriolytic action mechanism of cationic lignin is largely missing while it is critical to establish cationic lignin as a high-potential, low-cost, non-toxic, and biorenewable antimicrobial material.

To address these needs, in this work, we rendered cationic functionalities to alkali lignin (AL) *via* ring-opening reaction and investigated the antimicrobial efficacy of this cationic lignin (QAL) and AL against wild-type and kan-resistant *E. coli*. The quaternization of lignin to yield QAL was done in water ensuring a green synthesis of antimicrobial agents. We observed a strong bacteriostatic as well as bactericidal effect by using a relatively lower concentration of QAL (∼90% dead cells and ∼90−100% growth inhibition using 25−150 μg/mL of QAL for 1 h treatment). On the other hand, the non-cationic AL led to ∼20% growth inhibition, only emphasizing the importance of the cationization of lignin to achieve high antimicrobial efficacy. We measured the treatment-induced multimodal alterations of the bacterial cell envelope in detail using the ONPG test (membrane permeability), Nile Red test (exposure/loss of lipid from cell envelope), atomic force microscopy (cell roughness), and scanning electron microscopy (loss of cell integrity and intercell aggregation) imaging. We also studied how electrostatic interactions drove the adsorption of QAL onto the bacterial outer cell envelope. This comprehensive investigation of the antimicrobial action mechanism reveals the route to the effectiveness of QAL. Finally, we showed that QAL was not cytotoxic against human embryonic kidney cells up to a concentration at which QAL showed maximum antimicrobial activities. Together, our efforts potentially hinted toward high efficacy, affordable antimicrobial solutions for preventing pathogenic bacterial (including ESKAPE) infections, designing antimicrobial coatings for healthcare equipment/food processing lines, disinfecting water, and so on with the least cytotoxicity.

MATERIALS AND METHODS

Materials. For QAL synthesis, alkali lignin (AL) (source: Norway spruce, product number 370959, Millipore Sigma, St. Louis, MO), glycidyl trimethyl ammonium chloride (GTMAC) (Millipore Sigma, St. Louis, MO), sodium hydroxide (TCI, Portland, OR), and dialysis membrane (Spectra/Por 6 Dialysis Tubing, 1kD, 45 mm, 33 ft) (Repligen, Waltham, MA) were used as received.

To evaluate antimicrobial performance, the wild-type *E. coli* (DH10B) strain was obtained from New England Biolab (Ipswich, MA), and the kanamycin-resistant (kan-resistant) *E. coli* strain (SSBIO009) was transformed as described in the Supporting Information (Table S2) and prior literature.[79] For bacteria culture and antimicrobial assays, Luria Bertani (LB) broth (Miller) (AMERSCO, Solon, OH), bacteriological grade agar (Lab Scientific, Highlands, NJ), kanamycin sulfate (Teknova Inc., Hollister, CA), and 10× phosphate buffer (PBS, Fisher Scientific, Hampton, NH) were purchased and used. In addition, Nile Red (Santa Cruz Biotechnology Inc., Dallas, TX), ortho-nitrophenyl-β-D-galactopyranoside (ONPG) (Sigma-Aldrich, St. Louis, MO), and glutaraldehyde (Sigma-Aldrich, St. Louis, MO) were acquired. To measure the O.D. of bacterial suspensions and absorbance in the ONPG test, 96-well plates (Greiner Bio-One μClear Bottom 96-Well Polystyrene Microplates) were used.

For the cytotoxicity study, the human embryonic cell line (HEK293) was obtained from Synthego (Redwood City, CA). The following media and reagents were also purchased: Dulbecco's modified Eagle medium (DMEM) (Cytiva, Marlborough, MA), fetal bovine serum (FBS) (Fisher Scientific, Waltham, MA), 100× Penicillin/Streptomycin (Cytiva, Marlborough, MA), and CCK-8 kit (Dojindo, Rockville, MD).

Lignin-Based Cationic Antimicrobial (QAL) Synthesis and Characterization. The alkali lignin (AL) was quaternized following a protocol similar to the prior literature.[80] Briefly, 1 g of alkali lignin was dissolved into 100 mL of deionized water by adjusting the pH to 12.5 using NaOH. The temperature of this aqueous lignin solution was adjusted to 70 °C. After that, 1.7 mL of GTMAC was gradually added to the lignin solution with a constant stirring speed of 100 rpm. The reaction took place for 1 h under an N_2 environment. The product mixture was cooled down in a water bath followed by a pH adjustment to 7 with 0.25 M H_2SO_4. The mixture was dialyzed for 48 h using dialysis membranes (MWCO 1 kDa). The remaining product in the dialysis pouch was taken out and dried in a vacuum oven at 70 °C overnight to yield QAL (∼45%) as a brown powder.

To confirm the quaternization of lignin, ^{1}H nuclear magnetic resonance (^{1}H NMR) spectra (Figure S1) of alkali lignin, GTMAC, and QAL were acquired using a Bruker Avance III-HD 400 NMR spectrometer. Deuterated dimethyl sulfoxide (d-DMSO) and deuterated deuterium oxide (D_2O) were used as solvents for alkali lignin and QAL, respectively. Fourier transform infrared spectroscopy (FTIR) analysis of AL and QAL (Figure 1) was conducted using a Nicolet iS50 FTIR Spectrometer with an ATR accessory. The scans (32/sample) were done in the wavenumber range of 400−4000 cm^{-1}. Furthermore, the charged states of the QAL at different pH values (∼2−10) were evaluated using a ZetaPALS analyzer (Brookhaven Holtsville, NY) following established protocols.[81,82,74] The pH values of QAL solutions (0.2 mg/mL) were adjusted using 0.1 M H_2SO_4 and 0.1 M NaOH. Please see the Supporting Information for the experimental details of ^{31}P NMR (Figure S2) to obtain compositions of AL[83,84] and QAL (Table S3), X-ray photoelectron spectroscopy (Figures S3 and S4, Table S4), and ion exchange capacity (IEC) determination (eq S1) of QAL.

Bacterial Culture. The wild-type and kan-resistant *E. coli* strains were cultured in liquid LB media (25 g of LB in 1 L of sterilized water) or on solid agar plates (25 g of solid LB and 15 g of agar powder dissolved in 1 L of sterilized water). In each case, the media used for culturing kan-resistant *E. coli* were supplemented with 30 μg/mL of kanamycin to ensure only kan-resistant bacteria were yielded.[85] For solid agar plate-based studies, the *E. coli* strains (stock stored in glycerol) were streaked on solid agar plates. The streaked plates were incubated at 37 °C overnight. After that, a single colony from this agar plate was selected, transferred, and incubated in 4 mL of liquid LB media at 37 °C overnight with 250 rpm of agitation. Before the antimicrobial treatment of the bacteria grown in liquid LB, the bacteria cells were centrifugated, washed twice, and resuspended in 5 mM PBS buffer. The cell concentration in PBS buffer was then adjusted to 1.6×10^8 cells/mL (corresponding to OD_{600} of ∼0.2)[10] for further antimicrobial treatment.

Live/Dead Assay. The live/dead BacLight bacterial viability kit (Thermo Fisher Scientific, Waltham, MA) was used for flow cytometry measurements and confocal laser scanning microscopy (CLSM) imaging.[86] In particular, green fluorescence (SYTO9) is identified for bacteria cells that are intact, while the cells with compromised membranes are considered dead and identified as red (propidium iodide, PI). Briefly, wild-type and kan-resistant *E. coli* were grown in LB for 8 h. After that, the OD_{600} was adjusted to 0.2 in PBS. The cells were treated with QAL (0−300 μg/mL) for 1 h. The cells were harvested by centrifugation at 10,000*g* for 3 min, resuspended, and washed two times with NaCl (0.85 wt % in DI water). For flow cytometry measurements, 10 μL of cells (concentration adjusted to OD_{600} of ∼0.125) was mixed with 987 μL of 0.85 wt % NaCl. 3 μL of a mixture of SYTO9 and PI (1:1 v/v) was then added to the cell suspension and incubated in the dark for 15 min. A flow cytometer, BD FACSAria II (Franklin Lakes, NJ) at

https://doi.org/10.1021/acssuschemeng.3c01414
ACS Sustainable Chem. Eng. 2023, 11, 10364−10379

the Nebraska Center for Biotechnology, was used to determine the amount of dead and live cells.

Furthermore, for CLSM imaging, the NaCl-washed cells (untreated and treated kan-resistant *E. coli* strains) were resuspended in 200 μL of 0.85 wt % NaCl ($OD_{600} \approx 1$). In a separate vial, 6 μL of each dye, SYTO9 and PI, was mixed in 1 mL of the 0.85 wt % NaCl solution. 10 μL of each bacterial suspension and 10 μL of the dye mixture were then placed on the top of glass slides.[87] The cells were allowed to stain on these glass slides in the dark for 15 min. After that, the stained cells on glass slides were covered with coverslips and observed under a CLSM (Nikon A1R-Ti2). The excitation/emission maxima were 480/500 nm for SYTO9 and 490/635 nm for PI, respectively.[86]

Colony-Forming Unit (CFU) Reduction Assay. The antimicrobial performance of QAL was also studied using the colony forming unit (CFU) assay. The bacterial strains were treated with QAL in both PBS and LB. Briefly, both strains were treated with 0, 25, 50, 75, 100, 150, 200, and 300 μg/mL final concentrations of QAL in 5 mM PBS/LB with a treatment time of 1 h. After that, each bacterial suspension was diluted twice (100 times) in 5 mM PBS/LB. 5 μL of each final dilution, for wild-type and kan-resistant *E. coli*, was then placed on top of agar plates and spread in all directions. The plates were incubated at 37 °C for 15 h.[10,23] Finally, the cells were counted, and the % CFU reduction was calculated with eq 1 for three repetitions.

$$\%\text{CFU reduction} = \frac{\text{CFU}_{\text{untreated } E.coli} - \text{CFU}_{\text{treated } E.coli}}{\text{CFU}_{\text{untreated } E.coli}} \times 100\% \quad (1)$$

To show how the quaternization (in QAL) elevates the antimicrobial performance, we also performed the CFU reduction assays for AL in a similar manner, but by dissolving AL in appropriate solvents. Since AL can be dissolved in both organic solvent (DMSO) and water at alkaline pH, we studied CFU reduction of AL upon dissolving it in both 15% (v/v) DMSO and DI water with elevated pH (10.3, using NaOH). These samples were named AL-DMSO and AL-NaOH, respectively.

Zeta Potential Measurement. The charge interactions between QAL and bacteria were probed by zeta potential measurements. Here, wild-type and kan-resistant *E. coli* ($OD_{600} \approx 0.2$) were treated with different concentrations of QAL (0−300 μg/mL) for 5 min, 30 min, 1 h, and 2 h. The treated cells were centrifugated at 4700 rpm for 15 min, washed twice with DI water, and then resuspended in DI water for zeta potential measurements.

Adsorption Isotherm. To study the adsorption of QAL (adsorbate molecules) onto the wild-type and kan-resistant *E. coli* cells (adsorbent surface),[88] protocols described in the prior literature were followed.[89] Briefly, 900 μL of each bacterial suspension ($OD_{600} \approx 0.2$, equivalent to 1.6×10^8 cells/mL) was mixed with 100 μL of QAL to obtain different final concentrations of treatment solution ($C_0 \approx 25-200$ μg/mL).[89,90] The mixtures were incubated for 1 h at 37 °C and 250 rpm (antimicrobial treatment conditions). After that, the samples were frozen in an ice bath followed by centrifugation for 15 min at 4700 rpm.[89] After centrifugation, the supernatant was collected (containing unadsorbed QAL). 200 μL of this supernatant from each type of treatment was placed in separate wells of a 96-well plate, and their absorbance was measured at 350 nm to determine the residual concentration of QAL in the supernatant (C_{sup}). The QAL concentration in the supernatant (C_{sup}) was measured using a calibration curve (Figure S5) constructed to show the absorbance of QAL at 350 nm as a function of its concentration. While developing this calibration curve, the background absorbance (from the 96-well plate and water without sample) was subtracted from the measured absorbance in each case.

To study how the adsorbate (QAL) adsorbs onto bacteria, the collected data (C_{sup}, q_{ads}) were fitted with the linearized forms of Langmuir,[91,92] Freundlich,[93] and Temkin[94−96] isotherms representing monolayer (Langmuir)/multilayer (Freundlich) adsorption, and the effects of adsorbate-adsorbent interactions (Temkin), respectively.[90,97,98] The details of isotherm equations (eqs S2−S5) and respective fit parameters are shown in Table S5 of the Supporting Information.

Nile Red Staining. Nile Red, a lipophilic stain, (Santa Cruz Biotechnology Inc., Dallas, TX), was used to determine whether the lipid layers of treated cells were exposed. To do so, an established protocol was followed.[11] Briefly, 900 μL of *E. coli* ($OD_{600} \approx 0.2$) were treated with 0−300 μg/mL of QAL for 5 min and 1 h. The cells were harvested by centrifugation (4700 rpm for 15 min) and washed twice with 5 mM PBS. 2 μL of 25 mM Nile Red solution in DMSO was added to each of the 1 mL cell suspensions and incubated for 3 h in the dark. The stained cells were harvested by centrifugation (4700 rpm, 15 min), washed twice in 5 mM PBS, and resuspended in 200 μL of the same buffer. For the fluorescence measurements, the samples were placed in a 96-well plate, and the fluorescence was measured in a microplate reader. On the other hand, for the CLSM imaging, 10 μL of the kan-resistant *E.coli* strain, treated for 5 min in QAL solution with different concentrations, was added on top of glass slides, covered with coverslips, and observed under CLSM (Nikon A1R-Ti2). The excitation and emission maxima for Nile Red were 560 and 570−620 nm, respectively.

Inner Membrane Permeability. The inner membrane permeability of *E. coli* was assessed by the release activity of β-galactosidase. This enzyme release was probed using ONPG (*o*-nitrophenyl-β-D-galactopyranoside). If the inner membrane is disrupted by the action of QAL, ONPG will be hydrolyzed by β-galactosidase producing *o*-nitrophenol (absorbance∼420 nm).[99] Shortly, the cell suspensions, grown in LB for 8 h, were adjusted to $OD_{600} \approx 0.2$ in a solution of 1.5 mM ONPG in 10 mM PBS (pH 7.2).[100] In a 96-well plate, 200 μL of the cell suspension was mixed with QAL (final concentration of 0−300 μg QAL/mL). The absorbance was measured at 420 nm over 2 h.

Atomic Force Microscopy (AFM) Imaging. To understand the nature of morphological changes/damages on bacteria caused by QAL, AFM imaging (MFP-3D-Bio AFM; Oxford Instruments Asylum Research, Santa Barbara, CA) of untreated and QAL-treated cells was performed. Briefly, the cell suspension ($OD_{600} \approx 0.2$) was treated with 0−300 μg/mL of QAL for 1 h. After that, the cells were harvested by centrifugation at 4700 rpm for 15 min and washed twice with DI water. The final pellet was resuspended in DI water. 20 μL of each suspension was transferred on the top of ethanol-cleaned glass slides and allowed to dry in a desiccator with an N_2 atmosphere overnight. Tapping-mode AFM imaging at a scan rate of 0.2 Hz and 256 scanning lines were performed with an AC240TS silicon cantilever (nominal spring constant of 10.06 N/m, nominal tip radius of 7 nm) (Olympus Micro cantilevers, Tokyo, Japan). To measure the surface roughness from AFM height images across 200 nm^2 regions of not less than 10 bacterial cells, Igor Pro 15 software was used.[11] The statistical difference between untreated and treated wild-type and kan-resistant *E. coli* cells was determined by performing Student's *t*-test.

Scanning Electron Microscopy (SEM) Imaging. To confirm the morphological alterations of bacteria upon QAL treatment, SEM imaging was conducted (Helios NanoLab 660). The cell suspensions of wild-type and kan-resistant *E. coli* ($OD_{600} \sim 0.2$) were treated with 0−300 μg/mL of QAL for 1 h. After that, the cells were harvested by centrifugation at 4700 rpm and washed twice with PBS. Bacterial cells were fixed in glutaraldehyde (2.5 vol % in 5 mM PBS) for 4 h at 4 °C and dehydrated sequentially with 20, 30, 70, 90, and 100 vol % ethanol (10 min in each case).[101] Before imaging, the bacteria samples were coated with platinum-palladium for 90 s.

Transmission Electron Microscopy (TEM) Sample Preparation. The cell suspensions of kan-resistant *E. coli* ($OD_{600} \approx 0.2$) were treated with 0, 25, 150, and 300 μg/mL QAL for 1 h. After that, the cells were harvested by centrifugation at 4700 rpm and washed twice with PBS. The cells were fixed and post-fixed with 2.5 vol % glutaraldehyde and 1 vol % osmium tetroxide, respectively. Sequential dehydration processes were conducted with 30, 50, 75, 95, and 100% ethanol and lastly with acetone. The samples were embedded in resin blocks (Spurra's kit (Electron Microscopy Sciences, Hatfield, PA)). After that, the resin blocks were cross-sectioned with a thickness of 100 nm using a Leica EM UC7 ultramicrotome. Finally, the thin sections were stained using uranyl acetate and lead citrate, mounted

https://doi.org/10.1021/acssuschemeng.3c01414
ACS Sustainable Chem. Eng. 2023, 11, 10364−10379

on copper grids (Ted Pella), and observed under TEM (Hitachi H7500).

Cytotoxicity Assay. Human embryonic kidney cells (HEK293) were cultured in Dulbecco's modified Eagle medium (DMEM), a high glucose medium supplemented further with 10% fetal bovine serum (FBS) and 1× penicillin/streptomycin antibiotic. 25,000 cells were seeded in each well of a 96-well plate and allowed to grow overnight in a humidified CO_2 incubator at 37 °C and 5% CO_2 levels. Cells were treated with AL and QAL (25−1000 μg/mL) for 48 h. Here, the concentrated stock solution of AL was prepared with 15% DMSO in DI water (v/v) first, which was further diluted with DMEM to the desired polymer concentration and added to the cell suspension in the well plates subsequently. On the other hand, the QAL stock solution was prepared with DI water and diluted to the same extent as was done for AL. To understand the effect of DMSO−water on cell viability, we also performed a cytotoxicity assay with 15% DMSO in water (without polymer). After 48 h of incubation of HEK293 cells in AL, QAL, or DMSO-water, media were removed, and 100 μL of diluted CCK-8 reagent (as per manufacturer's instruction) was added in each well of the 96-well plate and placed in the CO_2 incubator for another 4 h. 50 μL solution from each well was then added to a fresh 96-well plate along with 50 μL of DI water. Absorbance readings from the 96-well plate were taken using a multimode reader at 450 nm, and the %cell viability was calculated using the following equation:

$$\%\text{cell viability} = \frac{\text{treatment absorbance} - \text{background absorbance}}{\text{control absorbance} - \text{background absorbance}} \times 100 \quad (2)$$

For all the experiments, DI water-treated cell samples were considered as control, and the corresponding absorbance was used as control absorbance. The absorbance of the CCK-8 reagent was used as background absorbance in the above equation.

RESULTS AND DISCUSSIONS

Synthesis and Characterization of QAL. In order to develop inexpensive and sustainable antimicrobial materials to fight against antibiotic resistance, we used commercially available alkali lignin (AL) from a plant source (Norway spruce, $M_n \approx 8564$ g/mol, $M_w \approx 21{,}795$ g/mol, PDI ≈ 2.54).[64] We chose this variant of lignin as it is commercially available in bulk amounts from a reliable source (Millipore-Sigma). We quantified the composition of this specific source of AL using ^{31}P NMR following an established protocol[84] (Figure S2, Table S3 in the Supporting Information): guaiacyl -OH: 2.02 mmol/g; syringyl -OH: 0.19 mmol/g; *p*-hydroxyphenyl -OH: 0. 38 mmol/g; total phenolic -OH: 4.24 mmol/g; aliphatic -OH: 2.33 mmol/g; -COOH: 0.41 mmol/g. This composition was in agreement with what was reported earlier by others[84] for the same source of AL (Table S3). To design antimicrobial materials, we rendered cationic functionalities to this AL *via* quaternization using glycidyl trimethyl ammonium chloride (GTMAC). The major steps of synthesizing the cationic lignin (QAL) (Figure 1a) were (i) solubilization of alkali lignin by adjusting its pH to 12.5 using NaOH, (ii) cationization of this solubilized lignin at 70 °C for 1 h in the presence of GTMAC where GTMAC-to-lignin mass ratio was maintained as 1.9: 1, (iii) cooling down the reaction products followed by neutralization of excess NaOH by adjusting the pH back to 7 using 0.25 M H_2SO_4, and (iv) purification of QAL using dialysis membranes (MWCO 1 kDa) for 48 h.

This quaternization process happened in water (no organic solvent) ensuring a green synthesis of the antimicrobial agent. The reaction conditions (pH, reaction temperature, time, GTMAC-to-lignin ratio, and lignin concentration in water) were chosen to selectively react GTMAC with the aromatic phenolic (-OH) groups of neutral lignin and achieve a water-soluble version of QAL[80] with minimal formation of undesired side products. In step (i), an alkaline pH was used as a pH >10 is required to solubilize alkali lignin and generate nucleophilic intermediates (i.e., deprotonation of -OH groups to give ($-O^-$) anions).[82,102−105] It has been reported that as compared to aliphatic -OH groups, the aromatic -OH groups (forming phenolate ($-O^-$) anions) of lignin are more prone to initiating the nucleophilic attack on GTMAC.[82,106] In this reaction, the nucleophilic intermediates of lignin attack and attach to the highly reactive epoxy groups of GTMAC *via* an oxirane ring-opening reaction and produce cationic QAL (Figure 1a, main reaction). Nonetheless, a few byproducts can also form due to the hydrolysis of GTMAC and QAL, taking place under highly alkaline conditions (Figure 1a, side reactions).[31,42,82] However, we used optimal conditions (70 °C and 1 h) for our quaternization reaction to minimize the formation of undesired side products. The optimal conditions were chosen based on a prior work,[82] which revealed that a temperature > 70 °C and reaction time > 1 h can promote the decomposition of GTMAC and QAL and reduce the yield of QAL. Another advantage we had was that the side product produced *via* hydrolysis of GTMAC was water-soluble and of low molecular weight. Thus, this cationic side product and unreacted GTMAC were easy to separate from QAL *via* dialysis.[82] The hydrolysis of QAL, another possible side reaction in this cationization process, was shown to be more probable in low-water systems.[106] To minimize this side reaction, we used a dilute solution of alkali lignin (1 wt % in water).[80]

We confirmed the quaternization of AL using ^{1}H NMR (Figure S1), ^{31}P NMR (Figure S2, Table S3), and FTIR (Figure 1b). ^{1}H NMR of QAL showed proton peaks at 3.2 ppm (-O-CH_2-CHOH-N($C\mathbf{H}_3$)$_3^+$) and 3.5 ppm (-O-CH_2-$C\mathbf{H}$OH-N(CH_3)$_3^+$ from its cationic side chains. These peaks were also present in cationic GTMAC, but not in non-cationic alkali lignin (Figure S1) (as expected), showing successful quaternation of AL to QAL. In addition, ^{31}P NMR indicated that the phenolic -OH content decreased from AL (4.24 mmol/g) to QAL (0.57 mmol/g) (Figure S2, Table S3). This confirmed that the cationization happened upon conversion of the phenolic -OH groups and corroborated with the literature.[82,106] FT-IR spectra (Figure 1b) also confirmed the successful attachment of quaternary amine groups to AL to give QAL. The IR peak at 1480 cm^{-1} (box a, Figure 1b) was assigned to symmetric -CH_3 stretching of cationic quaternary ammonium compounds and was only seen for cationic GTMAC and QAL but not for unmodified lignin (AL). Also, the peak at 928 cm^{-1} (box b in Figure 1b) was assigned to C−O stretching vibration of ether (in QAL) and epoxy ether (in GTMAC). This peak was not present in unmodified AL as expected. The elemental analysis using XPS (Figures S3 and S4) showed an increase in %N (2.38%) in the QAL sample from 0% in AL (Table S4), indicating successful quaternization of lignin.[19] The ion exchange capacity (IEC, mmol of quaternary ammonium groups/g of dry polymer) of QAL was also measured as 1.2 (see the Supporting Information for experimental details of IEC measurements).[64,107] We chose this specific IEC as it gave a water-soluble variant of QAL, a pre-requisite for antimicrobial studies in aqueous systems.

The zeta potential of pH-unmodified QAL (pH ∼ 5.7) was found to be +19.84 ± 0.99 mV (Figure 1c), which was consistent with a prior report (+21.7 ± 1.6 mV).[81] Also, QAL

https://doi.org/10.1021/acssuschemeng.3c01414
ACS Sustainable Chem. Eng. 2023, 11, 10364−10379

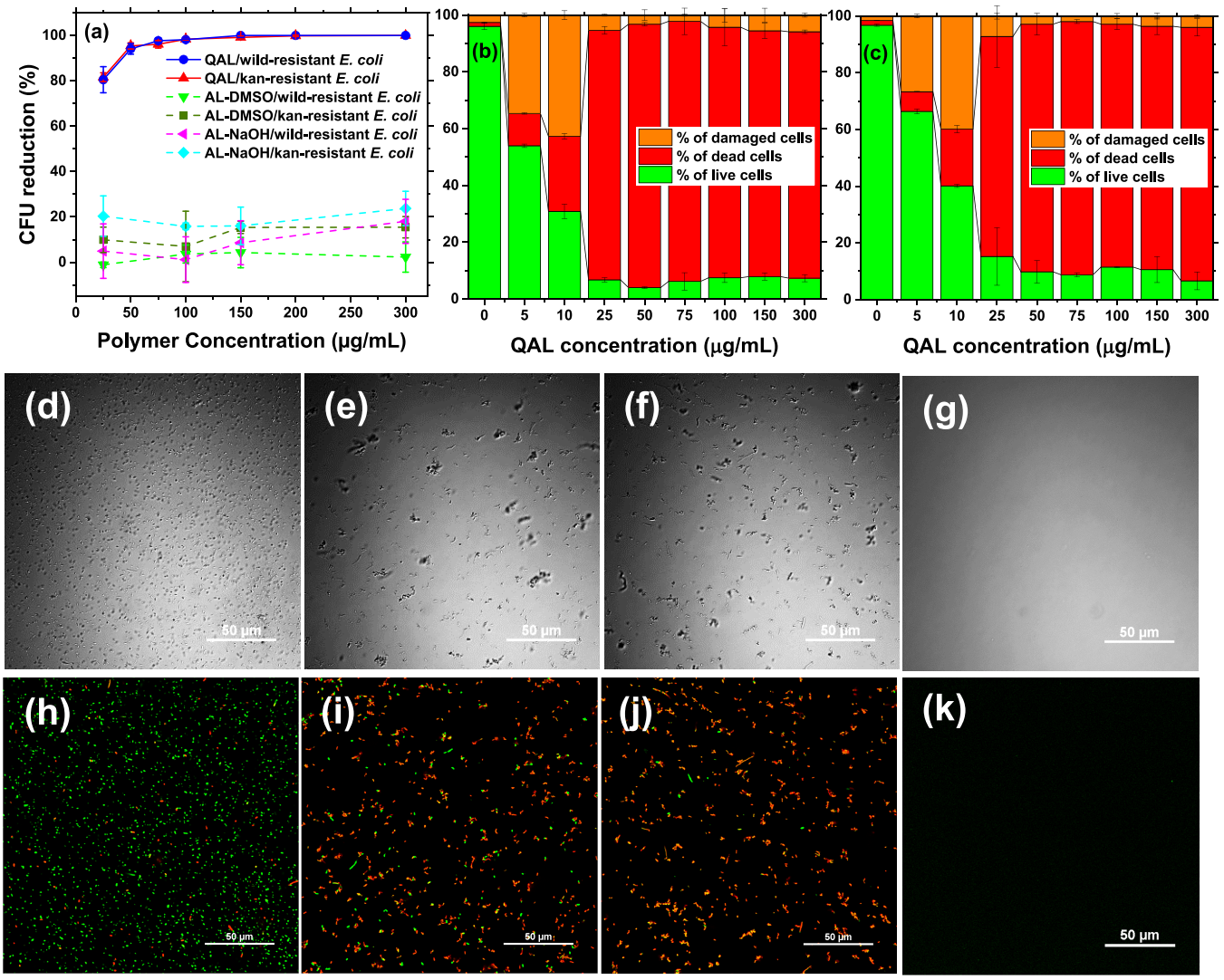

Figure 2. (a) % CFU reduction of wild-type and kan-resistant *E. coli* upon treatment with different concentrations of AL and QAL (25−300 μg/mL) for 1 h in 5 mM PBS buffer. Each data point and error bar represent the mean and standard deviation of 3 replicates, respectively. (b, c) Flow cytometry live/dead assay results of wild-type (b) and kan-resistant (c) *E. coli* cells treated with QAL (0−300 μg/mL) for 1 h in PBS buffer. Plots in panels (b) and (c) show the percentage of live, dead, and damaged cells counted after treatment. Each data point and error bar represent the mean and standard deviation of 2 replicates, respectively. (d−f) Bright-field and (h−j) fluorescence CLSM images of kan-resistant *E. coli*: untreated (0 μg/mL QAL) (d, h) and treated with 25 μg/mL (e, i) and 150 μg/mL (f, j) QAL for 1 h in PBS buffer. All the cells were stained with SYTO9 and PI dyes to differentiate between dead and alive cells. (g) Bright-field and (k) CLSM images of QAL after mixing with SYTO9 (green) and PI (red) dyes. All the images presented here were obtained by super-positioning both green and red color channels. The scale bars of bright-field and CLSM images panels (d)−(g) are 50 μm.

retained a similar positive potential over the wide ranges of pH (2−10) (Figure 1c), which corroborated the pH-insensitive nature of quaternary ammonium groups.[108] The positively charged nature of QAL, confirmed by zeta potential measurements, allowed QAL to interact with the net negatively charged cell envelope of bacteria (zeta potential ≈ −30 mV for both wild-type and kan-resistant *E. coli* with OD_{600} ≈ 0.2) (shown later in Figure 3a,b).

Antibacterial Activity of QAL. To evaluate the effect of cationic groups on the antimicrobial performance of lignin, we explored the antimicrobial efficacy (% CFU reduction) of both AL and QAL (Figure 2a). In these experiments, bacterial cells were treated first with AL or QAL in 5 mM PBS buffer for 1 h. After that, the cells were separated from the treatment solution *via* centrifugation, resuspended in PBS, and then transferred over the agar plates to grow for another 15 h. After 15 h, the colonies that formed on the agar plates were counted to calculate % CFU reduction using eq 1. When the *E. coli* strains were treated with QAL in 5 mM PBS, ∼95% CFU reduction was achieved using ∼50 μg/mL of QAL against both wild-type and kan-resistant *E. coli* strains (Figure 2a). This value reached ∼100% when ∼150−300 μg/mL of QAL was used (Figure 2a). This supersedes the % CFU reduction reported in the literature for other cationic variants of lignin (57% with 10 mg/mL)[29] and is on par with the other antimicrobial-based treatments[10,21,28,29,40,42,109] done in PBS (Table S1). As compared to cationic QAL, the non-cationic AL even with a reasonably high concentration (25−300 μg/mL) led to only ∼20% CFU reduction (Figure 2a). The low effectiveness of non-cationic AL also agreed with the prior literature (% CFU reduction of ∼30%,[29] MIC of ∼0.5−100 mg/mL)[70,71] and

https://doi.org/10.1021/acssuschemeng.3c01414
ACS Sustainable Chem. Eng. 2023, 11, 10364−10379

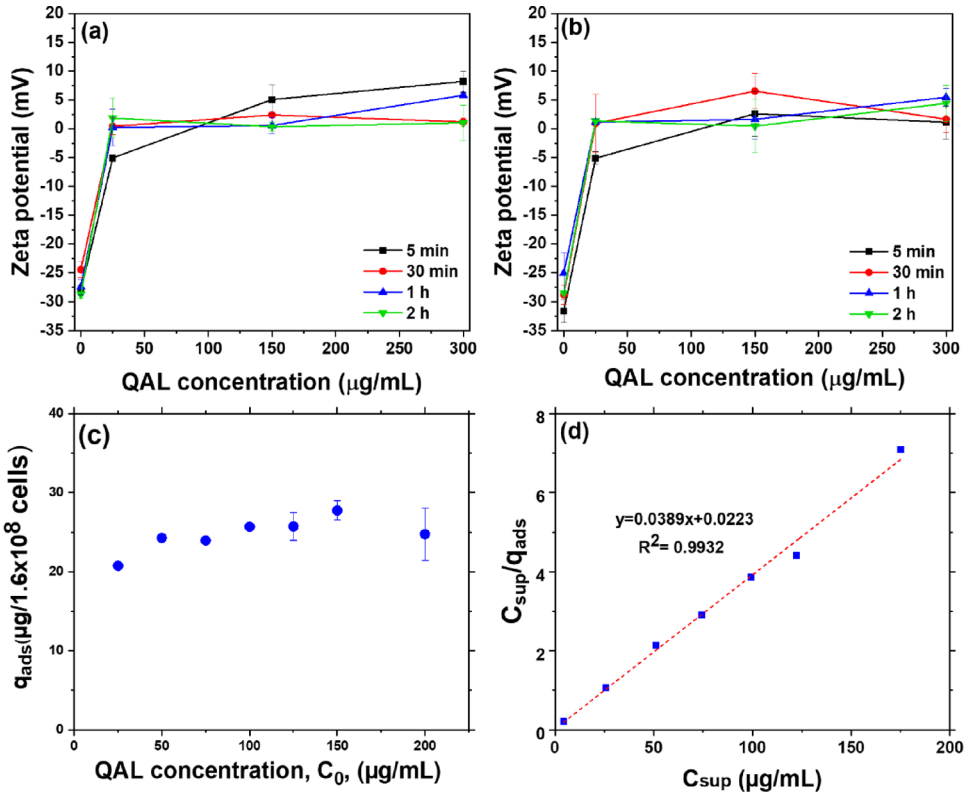

Figure 3. Change in zeta potential of (a) wild-type *E. coli* and (b) kan-resistant *E. coli* as a function of QAL concentration in treatment solution and treatment time. The treatment in both cases was done in 5 mM PBS after which the cells were transferred to DI water. (c) Amount of QAL adsorbed (q_{ads}) as a function of QAL concentration in treatment solution (C_0). The treatment time was 1 h. (d) Langmuir isotherm linearization for kan-resistant *E. coli*, where C_{sup} is the concentration of QAL in the supernatant separated from bacteria after treatment. Langmuir isotherm plot (d) was made based on eq S2, while the q_{ads} (c) was calculated based on eq S3. Each data point and error bar represent the mean and standard deviation of 3 replicates, respectively.

clearly pointed toward the role of cationic groups in QAL in elevating the antimicrobial efficacy of lignin.

The observations from live/dead assays (Figure 2b,c) were similar to what we saw in CFU reduction assays (Figure 2a). A 1 h-treatment with >25 μg/mL QAL killed ∼90% of the bacteria of both strains while causing damage to ∼4% more cells (Figure 2b,c). The dominance of dead cells demonstrated the bactericidal effect of QAL on both wild-type (Figure 2b) and kan-resistant (Figure 2c) *E. coli*. The features on the backbone and side chains of QAL together made it a strong bacteriolytic agent. Especially the cationic quaternary ammonium (QA) groups at the side chains of antimicrobials often tend to intercalate into and destabilize/disintegrate the lipid bilayer of the outer cell envelope of *E. coli*.[10,11,21,101,38] QAL does not only possess these cationic quaternary ammonium groups but also has a -CH_3/-OH group-rich lignin backbone[29] and hydrophobic alkyl side chains, which may have modulated the bacteria-polymer interactions and killing/growth inhibition of bacteria.

The findings from CLSM images of untreated (Figure 2d,h) and QAL-treated (Figure 2e,f,i,j) kan-resistant *E. coli* cells corroborated those from flow cytometry results (Figure 2c). For CLSM imaging, the cells were stained with SYTO9 and PI dyes after treatment with QAL. Both of these are DNA-intercalating dyes but STYO9 (green dye) can diffuse passively into living bacteria, while PI (red dye) cannot pass an intact bacterial membrane and only enters permeabilized dead bacteria.[110] Therefore, if the cells are predominantly green, it suggests that cells are alive, whereas if the cells are predominantly red, this likely suggests that the cell membrane is damaged allowing the permeation of the red dye. On the other hand, if the cells are orange, a partial damage of the cells allowing penetration of a few red dyes alongside green dyes can be inferred. In Figure 2h, the untreated cells were mostly green (indicating mostly alive cells) with only a few red, i.e., dead cells. When the bacteria cells were treated with QAL (Figure 2i,j), the cells looked mostly red and orange, suggesting that the cell membranes were compromised or damaged to different extents upon treatment with QAL. Just to rule out that the orange color in the images did not originate from any interaction between the dyes and QAL, we attempted to stain QAL (without bacteria) with both SYTO9 and PI. The CLSM image of this sample did not show any fluorescence (Figure 2k), supporting the non-interactive nature of QAL with both dyes.

So far, we have demonstrated the antimicrobial activities of QAL in PBS (5 mM). The antimicrobial studies in PBS/similar systems are important[11,18,23,32,38,62,101,111−115] since many industrial and environmental effluents may have salts (giving ionic strength) but not necessarily have energy sources as is present in LB media, which if used, lets the bacteria grow during treatment. Considering the significance of both, here, we performed the CFU reduction assays in both PBS (Figure 2a) and LB (Figure S6a) using QAL. The protocols for CFU assays were similar in both cases. As opposed to treatment in PBS, when the bacteria were treated with QAL in LB, % CFU reduction significantly decreased (Figure S6a). Similar to what was reported in the literature for cationic lignin-based

https://doi.org/10.1021/acssuschemeng.3c01414
ACS Sustainable Chem. Eng. 2023, 11, 10364−10379

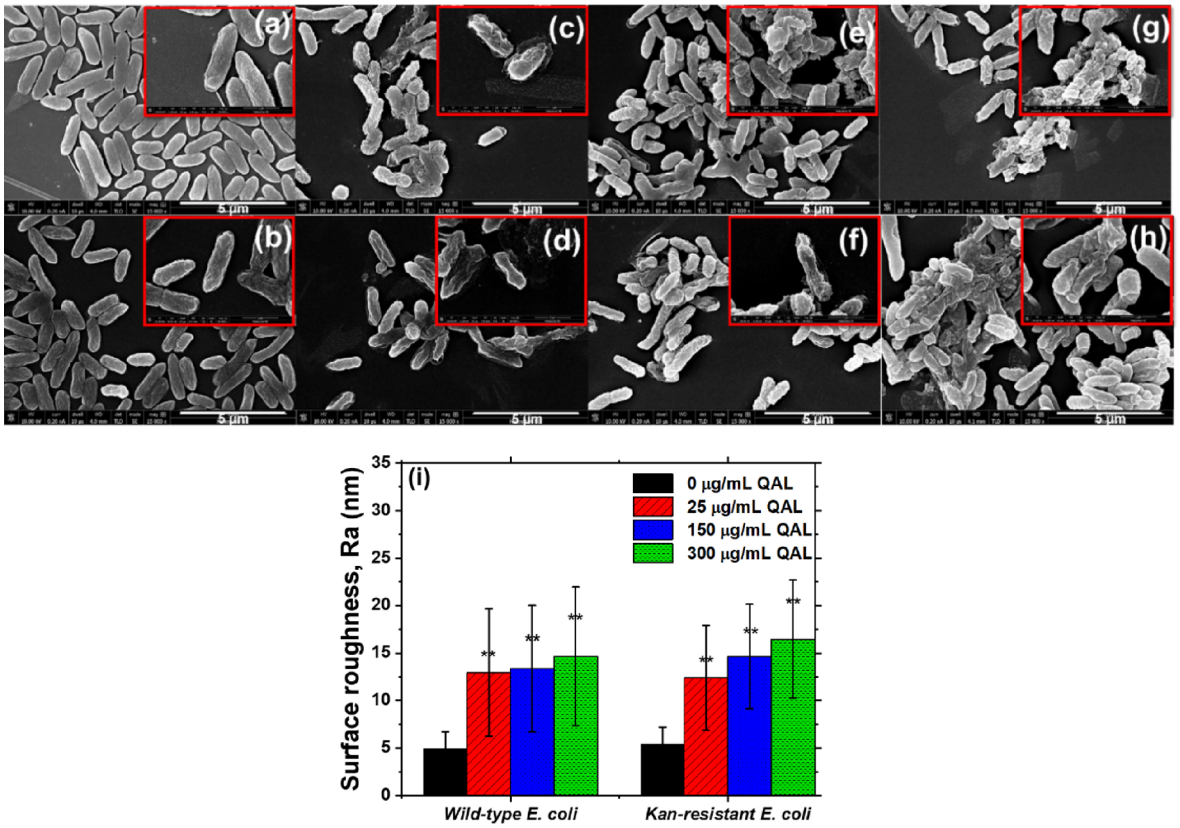

Figure 4. SEM images of wild-type and kan-resistant *E. coli*, (a, b) untreated and (c, d) treated with 25 μg/mL QAL, (e, f) and 150 μg/mL QAL and (g, h) 300 μg/mL QAL for 1 h, respectively. (i) Average surface roughness values (with standard deviations) of untreated wild-type and kan-resistant *E. coli* cells (black) and treated with 25 μg/mL (red), 150 μg/mL (red), and 300 μg/mL (green) QAL. In the AFM height images (after first order flattening process), 30 (200 × 200 nm^2) regions were randomly selected on at least 10 cells and used for roughness measurement. An unpaired *t* test was used for calculating the *p* values. The symbol ** represents $p < 0.05$ when compared with untreated cells (*p* values of two data sets lower than 0.05 were considered statistically different). The error bars represent the standard deviations.

treatment in LB media,[69] about 30% CFU reduction was achieved using ~300 μg/mL QAL in LB, and the value did not increase any further when the concentration of QAL increased up to 2000 μg/mL (Figure S6a). The observations from live/dead assays were also similar, i.e., ~90% killing by >25 μg/mL QAL in PBS (Figure 2b,c) while max 35% killing by 300−2000 μg/mL QAL in LB (Figure S6b,c). This can be rationalized by two phenomena. First of all, the LB allowed the bacteria to grow continuously while QAL was in action to kill them. At the same time, LB screened the charges of bacteria more. As a result, QAL failed to interact with bacteria electrostatically. The charge screening effect was evident from the zeta potential of bacteria in PBS (−40 mV) and in LB media (−2 mV) in the absence of QAL. For many other antimicrobial molecules relying on electrostatic interactions, similar reduced antimicrobial efficacy was reported in LB media compared to that in low-ionic strength systems.[10,116,117] These suggested that while demonstrating antimicrobial activities, the choice of the medium needs critical consideration as it can overshadow the potential of antimicrobial materials.

Zeta Potential and QAL Adsorption onto bacteria. To demonstrate the dominant electrostatic interactions between bacteria and QAL, the zeta potential of bacteria was measured with and without treatment (Figure 3a,b). While in LB-based treatment, the antimicrobial process was jeopardized by the simultaneous re-growth of bacteria, in PBS-based treatment, it was not the case. Rather, a cell death of ~90% was achieved (Figure 2b,c), and during this process, the bacteria lost its negative charges and became neutral (0 mV when treated with 50 μg/mL of QAL) (Figure 3a,b). This indicated that the antimicrobial process was majorly driven by electrostatic adsorption of the incoming QAL on the surface of bacteria and neutralization of their surface charges. The zeta potential of the bacteria remained the same (i.e., zero) upon increasing the concentration of QAL, further suggesting that additional QALs were not sticking to bacteria. This hypothesis was proven by the adsorption studies where we found that when the QAL concentration in the treatment solution went above 25 μg/mL, there was no further increase in the amount of QAL adsorbed onto the surface of bacteria (q_{ads}) (Figure 3c). Also, the adsorption data fitted well with the Langmuir isotherm (eq S2, Figure 3d) as compared to other isotherms (Freundlich, Temkin, eqs S4 and S5) based on R^2 values (Table S5) and inferred monolayer adsorption of QAL onto bacteria.

The plateau in adsorption and zeta potential was unlike many other antimicrobials, which caused a continuous increase in the bacterial surface charge toward positive values upon increasing the concentration of those agents.[10,16,101,118−121] This likely suggested that only a fraction of the cationic charges of those reported charge-overcompensating agents were involved in attaching to bacteria leaving some unused positive charges of the agents on the bacteria surface. Those excess free charges might have led to extensive bacterial aggregation proven *via* SEM/AFM.[10] Our train of thought here is that if

https://doi.org/10.1021/acssuschemeng.3c01414
ACS Sustainable Chem. Eng. 2023, 11, 10364−10379

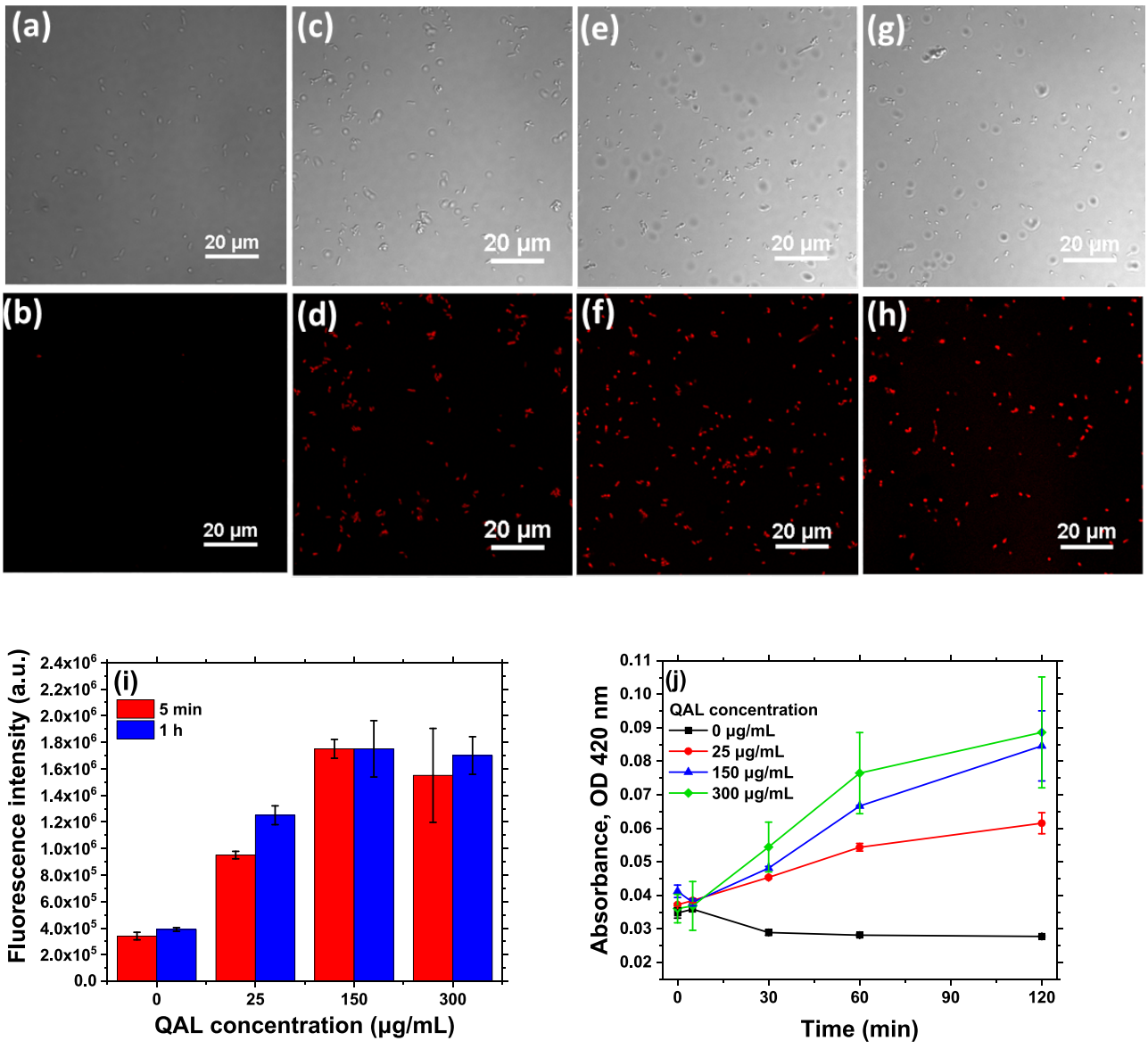

Figure 5. Bright-field and fluorescent CLSM images of kan-resistant *E. coli* cells untreated (a, b) and treated for 1 h with 25 μg/mL (c, d), 150 μg/mL (e, f), and 300 μg/mL (g, h) QAL. (i) Fluorescence signals from kan-resistant *E. coli* cells upon treatment with QAL (0−300 μg/mL) and staining with a Nile Red dye. The treatment time was varied from 5 min to 1 h. (j) ONPG-based study of inner membrane permeabilization of kan-resistant *E. coli* cells. The *y* axis shows the absorbance of *o*-nitrophenol (produced upon the reaction of ONPG with the enzyme (β-galactosidase) present in bacterial cytoplasm) at 420 nm. Here, the bacteria cells ($OD_{600} \approx 0.2$) were treated with 0−300 μg/mL QAL for 0−120 min. The error bars in the Nile Red staining test and ONPG test were estimated from standard deviations of 3 repeated sets of data.

the polymer chains are of high volume or bulky (like lignin), a lesser number of chains may be sufficient to cover the bacteria, leaving not many unused dangling charges of the antimicrobial agents to induce bacterial aggregation. The milder bacterial aggregation, seen in SEM images (Figure 4), thus supported the near-neutral surface charge and mono-layer-like low adsorption of QAL onto bacteria.

Morphological/Compositional Changes and Aggregation of Bacteria. Next, we visualized how the treatment with QAL altered the morphology and roughness of wild-type and kan-resistant *E. coli* using SEM (Figure 4a−h) and AFM (Figures S7 and S8 and Figure 4i). As expected, in the SEM images, the healthy *E. coli* cells (both wild-type and kan-resistant) retained rod-shape with rounded ends, and the cell surface looked smooth and intact (Figure 4a,b); however, treatment with QAL roughened the bacterial cell envelopes and led to a relatively weak aggregation of bacteria (Figure 4c−h). The increased surface roughness of bacteria (Figure 4i) was further confirmed *via* AFM height images (Figure S7). For example, the surface roughness was 5.41 ± 1.77 nm for untreated kan-resistant *E. coli* cells while the roughness increased to 12.40 ± 5.54 nm and 14.63 ± 5.51 nm as the bacteria were treated with 25 and 300 μg/mL of QAL, respectively (Figure 4i). In the case of wild-type *E. coli*, the roughness increased from 4.9 ± 1.76 nm (untreated) to 12.9 ± 6.71 nm (treated with 25 μg/mL of QAL). Bacterial surface roughening was often attributed to component loss from lipopolysaccharide layers or other processes.[11,122,123] The extent of membrane damage by QAL was thus revealed by the Nile Red assay and ONPG test (Figure 5).

Nile Red Assay. To visualize the damage in the cell envelope of kan-resistant *E. coli* caused by QAL, bacteria were

https://doi.org/10.1021/acssuschemeng.3c01414
ACS Sustainable Chem. Eng. 2023, 11, 10364−10379

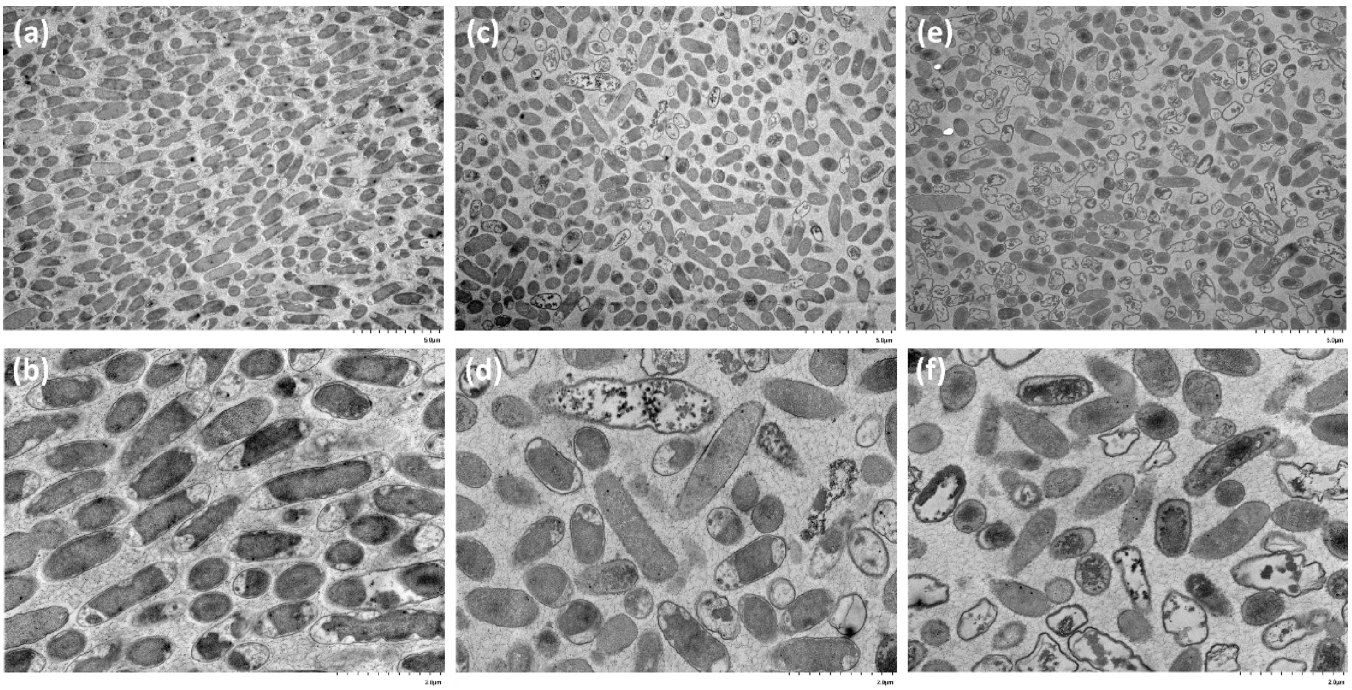

Figure 6. TEM images of kan-resistant *E. coli*, (a, b) untreated and (c, d) treated with 25 μg/mL and (e, f) 150 μg/mL QAL for 1 h. The scale bars for panels (a), (c), and (e) were 5 μm while they were 2 μm for panels (b), (d), and (f).

stained with Nile Red. In the Nile Red assay, the cells were treated first with QAL in PBS. After that, the cells were separated and re-suspended in DI water in which the Nile Red dye was added to stain the cells. Nile Red is a lipophilic dye[124] that selectively stains lipid-based components of the cell wall.[125,126] The outer membrane of an *E. coli* cell constitutes an (i) O-antigen, (ii) outer core, and (iii) inner core composed mostly of sugar-based hydrophilic compounds,[127,128,111,129−132] while the lipid A and phospholipid[133] underneath these layers generate the lipid bilayer. Therefore, when layers (i)−(iii) are damaged or compromised, exposing lipid regions underneath, Nile Red gets a chance to stain the lipids of the cell envelope and show red fluorescence.

In the Nile Red assay, most of the healthy cells showed no fluorescence (Figure 5a,b). This indicated that the lipid-based components in the cell membranes were intact and unexposed to Nile Red. However, treating these cells with just 25 μg/mL QAL for 5 min led to red fluorescence emission from the cells (Figure 5d,i). This clearly showed that a quick treatment with a low concentration of QAL was adequate to expose the lipid regions of bacteria. The zeta potential of bacteria also approached 0 mV upon a 5 min treatment with a similarly low concentration of QAL (Figure 3b). The simultaneous observations of charge neutralization and surface alteration suggested that the quick and effective damage was driven by an almost instantaneous electrostatic binding as QAL came in contact with bacteria. Comparing the bright-field (showing both damaged and healthy cells, Figure 5a,c,e,g) and fluorescence mode (showing damaged cells only in red, Figure 5b,d,f,h) images helped us to infer that the cell walls of almost all the cells were compromised, making Nile Red dyes reachable to lipids. Typically, in *E. coli* cells, the alteration or damage in the outer cell envelope is often induced by a coating of the outer cell envelope[10,11,134,135] or intercalation of backbone/side chains of antimicrobial molecules deep down into the lipid bilayers[10,11,14,101] followed by chain-induced pinning[14] of neighboring lipid layers, disrupted or loosened packing of lipids, lipid loss,[11] reduced mechanical properties,[11] and membrane destabilization thereby.[44,45] It was, however, not clear in our case whether the lipids were detached from the cell wall or just got exposed to Nile Red as we did not observe any extracellular vesicle formation (AFM, Figure S8), often attributed to electrostatic complexation between cationic antimicrobials and phospholipids detached from bacteria.[11]

Inner Membrane Permeabilization. To reveal whether the damage is simply external (i.e., on the cell envelope) or both external and internal, we also studied the inner membrane permeability *via* the ONPG test (Figure 5j). Briefly, ONPG is a substrate for β-galactosidase, a cytoplasmic enzyme. This enzyme would leak through the inner membrane of the cell wall when the membrane is disrupted. The leaked enzyme hydrolyzes ONPG into *o*-nitrophenol, which shows absorbance at 420 nm.[136−138] Therefore, an increase in absorbance of *o*-nitrophenol would indicate increased permeability of the inner membrane of bacteria cells. We treated the kan-resistant *E. coli* cells with 0−300 μg/mL QAL and the treatment time was varied from 0 to 120 min. The QAL treatment induced membrane permeabilization, which was evident from the higher absorbance at 420 nm in the case of QAL-treated cells compared to untreated cells (Figure 5j). With higher QAL concentration and higher treatment time, an increased amount of leakage of cytoplasmic β-galactosidase enzyme was evidenced. A comparison of the Nile Red staining test and ONPG test suggested that a 5 min treatment was adequate to cause damage to lipids of the cell envelope (Figure 5i) but was not enough to initiate inner membrane permeabilization (Figure 5j). This pointed toward the fact that the damage of the cell envelope was almost an instantaneous process, but the inner membrane permeabilization/leakage was a time-dependent process.

While the ONPG and Nile Red assays indicated the damage to the cell envelope and leakage from the cell cytoplasm, we

https://doi.org/10.1021/acssuschemeng.3c01414
ACS Sustainable Chem. Eng. 2023, 11, 10364−10379

did not see any evidence of alteration of proteins in bacteria upon QAL treatment. The gel electrophoresis of proteins extracted from both untreated and QAL-treated kan-resistant cells did not show any significant difference in protein bands (Figure S9), suggesting that the proteins did not degrade upon treatment (seen in some other antimicrobial agents),[50] nor did the bacteria produce any protein with different MW. This supported the hypothesis that QAL acts by non-specific binding-induced alterations rather than altering the protein profile of bacteria. This mechanism is ideal to treat a kan-resistant *E. coli*, the protein synthesis pathways of which are difficult to attack.

The fact that leakage is dependent on the concentration of the antimicrobial agent was also supported by TEM images (Figure 6). When kan-resistant *E. coli* were treated with just 25 μg/mL QAL (Figure 6c,d), bacteria cells were seen as coated with polymers. As the concentration of QAL increased, more cells appeared to be leaking as the interior of more cells started to look empty (Figure 6a,c,e), but the thickness of the polymer coating did not change significantly (matched with adsorption study and Langmuir-like monolayer coverage, Figure 3c,d). At the same time, the zeta potential of the cells did not increase further when the QAL concentration was increased beyond 25 μg/mL (Figure 3a,b). No significant increase in polymer coating and zeta potential with increasing concentration of QAL suggested that at high concentration, rather than sticking to the bacteria surface, the extra QAL may have acted by a needle-like poking effect (possibly through its quaternized side chains) that increased the cells leakage (Figure 5j).

Cytotoxicity Studies. We studied the viability of human embryonic kidney (HEK293) cells upon treatment with AL and QAL (Figure 7). Cationic QAL was not/minimally

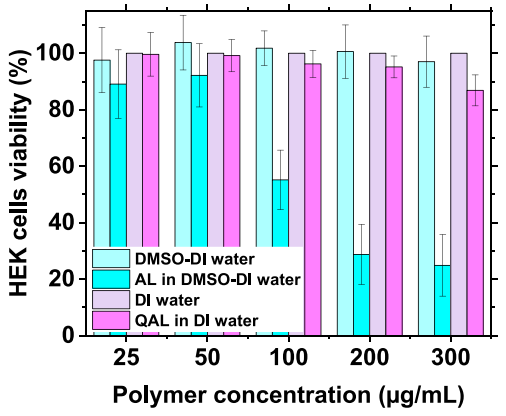

Figure 7. Cytotoxicity studies of AL and QAL against human embryonic kidney (HEK293) cells. DI water-treated cell samples were considered as control for % cell viability measurements in all cases.

cytotoxic against HEK293 cells (90−100% cell viability) up to a concentration range (0−300 μg/mL), in which QAL achieved 100% CFU reduction. On the other hand, non-cationic AL caused a significant reduction in cell viability. Since AL stock solutions to measure cell viability were made with 15% DMSO in water, we wanted to check the effect of DMSO on cytotoxicity and thus treated the cells with just DMSO−water (without AL). Interestingly, DMSO-treated HEK293 cells maintained high viability ruling out the effect of DMSO on cytotoxicity when treated with AL. While looking into the origin of different levels of cytotoxicity of AL and QAL, we found in the literature that most of the human cells actively maintain a slightly positive or charge-neutral state,[139] which may have modulated the interaction of cells with cationic QAL (repulsive interactions) and non-cationic AL (hydrophobic interactions). Last but not least, prior systematic studies on other classes of antimicrobials[38] suggested that the lengths of alkyl side chains (7.4 Å) and alkyl substitutes (1.48 Å) at the terminal of cationic sites of our QAL had the right balance to be highly antimicrobial while being non-toxic to human cells. This justified the high human cell viability against QAL observed experimentally.

SUSTAINABILITY ASPECT OF THIS WORK

Overall, these results pointed toward the high efficacy of cationic lignin-based antimicrobial agents. By tweaking lignin's chemical functionalities and optimizing the treatment mode and time, QAL can both kill and inhibit the growth of antibiotic-resistant bacteria efficiently. By converting an untapped agricultural/process waste, like lignin into value-added antimicrobials, we can significantly lower the expense of antimicrobial treatments/coatings in large-scale applications. Especially the potential of lignin-based antimicrobials in killing/inhibiting the growth of antibiotic-resistant strains can be leveraged to fight effectively against antibiotic resistance, ESKAPE pathogens, hospital-acquired infections, and treat hospital−/municipal wastewater without significantly impacting the aquatic environment. From a broader perspective, sustainable, scalable production of low-cost, efficient antimicrobials from waste lignin can help to sustain pulp and paper industries, biorefineries, and agricultural farms and support bioeconomy.

CONCLUSIONS

Through an extensive investigation of the antimicrobial nature of QAL and its impact on wild-type and kan-*resistant E. coli*, we demonstrated the high promise of QAL as an important class of biorenewable-based antimicrobial material. The live/dead assay revealed that a treatment with >25 μg/mL QAL for 1 h killed ∼90% of the bacteria cells and caused damage to ∼4% more cells. Remarkably, the growth of wild-type and antibiotic-resistant strains was inhibited at a similarly high level (∼90−100% CFU reduction using ∼25−150 μg/mL QAL). QAL did not only target, roughen, and damage the bacterial outer membrane (Nile Red) but also caused leakage from the cell cytoplasm (ONPG test). A Langmuir monolayer coverage of QAL onto bacteria was identified. The extensive investigation suggested that the electrostatic binding and cell envelope damage was almost instantaneous and complete with a low QAL concentration (25 μg/mL) in 5 min, while the leakage from the cell interior was dependent on the treatment time and concentration of QAL. Finally, QAL did not show any significant cytotoxicity against human embryonic kidney cells (HEK293). Altogether this work showed how QAL can play a critical role as a green, cost-competitive, scalable, and highly efficient antimicrobial with the capability of fighting against antibiotic resistance and supporting bioeconomy through a unique lignin valorization approach.

ASSOCIATED CONTENT

Supporting Information

The Supporting Information is available free of charge at https://pubs.acs.org/doi/10.1021/acssuschemeng.3c01414.

https://doi.org/10.1021/acssuschemeng.3c01414
ACS Sustainable Chem. Eng. 2023, 11, 10364−10379

Table reviewing antimicrobial agents reported so far, plasmid assembly, ^{1}H and ^{31}P NMR, XPS, IEC, live/dead assay in LB media, AFM, adsorption studies, SDS-PAGE, and relevant experimental details (PDF)

AUTHOR INFORMATION

Corresponding Author

Shudipto Konika Dishari − *Department of Chemical and Biomolecular Engineering, University of Nebraska-Lincoln, Lincoln, Nebraska 68588, United States;* orcid.org/0000-0003-1679-2332; Email: sdishari2@unl.edu

Authors

Karen Acurio Cerda − *Department of Chemical and Biomolecular Engineering, University of Nebraska-Lincoln, Lincoln, Nebraska 68588, United States*

Mark Kathol − *Department of Chemical and Biomolecular Engineering, University of Nebraska-Lincoln, Lincoln, Nebraska 68588, United States*

Gunjan Purohit − *Department of Biochemistry, University of Nebraska-Lincoln, Lincoln, Nebraska 68588, United States*

Ehsan Zamani − *Department of Chemical and Biomolecular Engineering, University of Nebraska-Lincoln, Lincoln, Nebraska 68588, United States*

Martha D. Morton − *Department of Chemistry and Nebraska Center for Integrated Biomolecular Communication, University of Nebraska-Lincoln, Lincoln, Nebraska 68588-0304, United States;* orcid.org/0000-0002-6411-1733

Oleh Khalimonchuk − *Department of Biochemistry and Nebraska Redox Biology Center, University of Nebraska-Lincoln, Lincoln, Nebraska 68588, United States; Fred & Pamela Buffett Cancer Center, Omaha, Nebraska 68198, United States;* orcid.org/0000-0002-3972-8678

Rajib Saha − *Department of Chemical and Biomolecular Engineering, University of Nebraska-Lincoln, Lincoln, Nebraska 68588, United States;* orcid.org/0000-0002-2974-0243

Complete contact information is available at: https://pubs.acs.org/10.1021/acssuschemeng.3c01414

Notes

The authors declare no competing financial interest.

ACKNOWLEDGMENTS

S.K.D. acknowledges the supports from the University of Nebraska Collaboration Initiative Grant and Voelte-Keegan Bioengineering Support Grant. E.Z. and S.K.D also acknowledge the supports from the U.S. Department of Energy (DOE), Office of Science, Basic Energy Sciences (BES) Early CAREER Award (#DE-SC0020336), NSF CAREER Award (#1750040), and the Nebraska Center for Energy Science Research (NCESR) Competitive Grant (Cycle 14) for the initial development of the project. K.A.C. thanks the Fulbright Scholars Program and the University of Nebraska Collaboration Initiative Grant for their supports. R.S. and M.K. acknowledge funding from the NSF CAREER Award (#1943310). O.K. acknowledges the supports from the National Institute of Health (NIH), the National Institute of General Medical Sciences (NIGMS) (#R35GM131701-01), and the University of Nebraska Research Initiative Grant. M.D.M. acknowledges the UNL Molecular Analysis and Characterization (MAC) Facility for NMR work and the Nebraska Center for Integrated Biomolecular Communication (NCIBC). A helium recovery system supporting the NMR spectrometers was purchased with support from the NCIBC Systems Biology Core (NIH NIGMS P20 GM 113126). The authors would like to acknowledge the help from Prof. You Zhou, Dr. Terri Fangman, and Dirk Anderson in acquiring the CLSM and TEM images as well as flow cytometry measurements at the Microcopy and Flow Cytometry Core Facilities of the Nebraska Center for Biotechnology. K.A.C. thanks Prof. Yinsheng Guo for the helpful discussion on the FT-IR analysis. The AFM and SEM imaging were performed at the UNL Nano-Engineering Research Core Facility (NERCF). Part of this research (XPS) was performed in the Nebraska Nanoscale Facility: National Nanotechnology Coordinated Infrastructure and the Nebraska Center for Materials and Nanoscience, which are supported by the National Science Foundation under Award ECCS: 2025298, and the Nebraska Research Initiative.

REFERENCES

(1) Tiihonen, A.; Cox-Vazquez, S. J.; Liang, Q.; Ragab, M.; Ren, Z.; Hartono, N. T. P.; Liu, Z.; Sun, S.; Zhou, C.; Incandela, N. C.; Limwongyut, J.; Moreland, A. S.; Jayavelu, S.; Bazan, G. C.; Buonassisi, T. Predicting Antimicrobial Activity of Conjugated Oligoelectrolyte Molecules via Machine Learning. *J. Am. Chem. Soc.* **2021**, *143*, 18917−18931.

(2) Tacconelli, E.; Carrara, E.; Savoldi, A.; Harbarth, S.; Mendelson, M.; Monnet, D. L.; Pulcini, C.; Kahlmeter, G.; Kluytmans, J.; Carmeli, Y.; Ouellette, M.; Outterson, K.; Patel, J.; Cavaleri, M.; Cox, E. M.; Houchens, C. R.; Grayson, M. L.; Hansen, P.; Singh, N.; Theuretzbacher, U.; Magrini, N.; Aboderin, A. O.; al-Abri, S. S.; Awang Jalil, N.; Benzonana, N.; Bhattacharya, S.; Brink, A. J.; Burkert, F. R.; Cars, O.; Cornaglia, G.; Dyar, O. J.; Friedrich, A. W.; Gales, A. C.; Gandra, S.; Giske, C. G.; Goff, D. A.; Goossens, H.; Gottlieb, T.; Guzman Blanco, M.; Hryniewicz, W.; Kattula, D.; Jinks, T.; Kanj, S. S.; Kerr, L.; Kieny, M. P.; Kim, Y. S.; Kozlov, R. S.; Labarca, J.; Laxminarayan, R.; Leder, K.; Leibovici, L.; Levy-Hara, G.; Littman, J.; Malhotra-Kumar, S.; Manchanda, V.; Moja, L.; Ndoye, B.; Pan, A.; Paterson, D. L.; Paul, M.; Qiu, H.; Ramon-Pardo, P.; Rodríguez-Baño, J.; Sanguinetti, M.; Sengupta, S.; Sharland, M.; Si-Mehand, M.; Silver, L. L.; Song, W.; Steinbakk, M.; Thomsen, J.; Thwaites, G. E.; van der Meer, J. W. M.; van Kinh, N.; Vega, S.; Villegas, M. V.; Wechsler-Fördös, A.; Wertheim, H. F. L.; Wesangula, E.; Woodford, N.; Yilmaz, F. O.; Zorzet, A. Discovery, Research, and Development of New Antibiotics: The WHO Priority List of Antibiotic-Resistant Bacteria and Tuberculosis. *Lancet Infect. Dis.* **2018**, *18*, 318−327.

(3) Moore, C. E. Changes in Antibiotic Resistance in Animals. *Science* **2019**, *365*, 1251−1252.

(4) Chang, Y.; Chusri, S.; Sangthong, R.; McNeil, E.; Hu, J.; Du, W.; Li, D.; Fan, X.; Zhou, H.; Chongsuvivatwong, V.; Tang, L. Clinical Pattern of Antibiotic Overuse and Misuse in Primary Healthcare Hospitals in the Outhwest of China. *PLoS One* **2019**, *14*, 1−12.

(5) Khan, F. A.; Söderquist, B.; Jass, J. Prevalence and Diversity of Antibiotic Resistance Genes in Swedish Aquatic Environments Impacted by Household and Hospital Wastewater. *Front. Microbiol.* **2019**, *10*, 1−12.

(6) Papajová, I.; Šmigová, J.; Gregová, G.; Šoltys, J.; Venglovský, J.; Papaj, J.; Szabóová, T.; Dančová, N.; Ihnacik, L.; Schusterová, I.; Sušinková, J.; Raková, J.; Regecová, I. Effect of Wastewater Treatment on Bacterial Community, Antibiotic-Resistant Bacteria and Endoparasites. *Int. J. Environ. Res. Public Health* **2022**, *19*, 2750.

(7) Evans, A.; Kavanagh, K. A. Evaluation of Metal-Based Antimicrobial Compounds for the Treatment of Bacterial Pathogens. *J. Med. Microbiol.* **2021**, *70*, No. 001363.

(8) Sánchez-López, E.; Gomes, D.; Esteruelas, G.; Bonilla, L.; Lopez-Machado, A. L.; Galindo, R.; Cano, A.; Espina, M.; Ettcheto, M.; Camins, A.; Silva, A. M.; Durazzo, A.; Santini, A.; Garcia, M. L.;

Souto, E. B. Metal-Based Nanoparticles as Antimicrobial Agents: An Overview. *Nanomaterials* **2020**, *10*, 292.
(9) Martinez-gutierrez, F.; Olive, P. L.; Banuelos, A.; Orrantia, E.; Nino, N.; Sanchez, E. M.; Ruiz, F.; Bach, H.; Av-Gay, Y. Synthesis , Characterization , and Evaluation of Antimicrobial and Cytotoxic Effect of Silver and Titanium Nanoparticles. *Nanomed.: Nanotechnol., Biol. Med.* **2010**, *6*, 681−688.
(10) Zamani, E.; Chatterjee, S.; Changa, T.; Immethun, C.; Sarella, A.; Saha, R.; Dishari, S. K. Mechanistic Understanding of the Interactions of Cationic Conjugated Oligo- and Polyelectrolytes with Wild-Type and Ampicillin-Resistant Escherichia Coli. *Sci. Rep.* **2019**, *9*, 1−12.
(11) Zamani, E.; Johnson, T. J.; Chatterjee, S.; Immethun, C.; Sarella, A.; Saha, R.; Dishari, S. K. Cationic Π-Conjugated Polyelectrolyte Shows Antimicrobial Activity by Causing Lipid Loss and Lowering Elastic Modulus of Bacteria. *ACS Appl. Mater. Interfaces* **2020**, *12*, 49346−49361.
(12) Li, X.; Bai, H.; Yang, Y.; Yoon, J.; Wang, S.; Zhang, X. Supramolecular Antibacterial Materials for Combatting Antibiotic Resistance. *Adv. Mater.* **2018**, *31*, 1805092.
(13) Scheberl, A.; Khalil, M. L.; Maghsoodi, F.; Strach, E. W.; Yang, J.; Chi, E. Y.; Schanze, K. S.; Reimhult, E.; Whitten, D. G. Quantitative Determination of Dark and Light-Activated Antimicrobial Activity of Poly(Phenylene Ethynylene), Polythiophene, and Oligo(Phenylene Ethynylene) Electrolytes. *ACS Appl. Mater. Interfaces* **2020**, *12*, 21322−21329.
(14) Wang, Y.; Chi, E. Y.; Schanze, S.; Whitten, D. G. Membrane Activity of Antimicrobial Phenylene Ethynylene Based Polymers and Oligomers. *Soft Matter* **2012**, *8*, 8547−8558.
(15) Guo, F. C.; Chen, C. Y. Zwitterionic Core-Sheath Nanofibers in Antibacterial Photodynamic Therapy. *ACS Appl. Polym. Mater.* **2022**, *4*, 4576−4587.
(16) Si, Z.; Li, J.; Ruan, L.; Reghu, S.; Ooi, Y. J.; Li, P.; Zhu, Y.; Hammond, P. T.; Verma, C. S.; Bazan, G. C.; Pethe, K.; Chan-Park, M. B. Designer Co-Beta-Peptide Copolymer Selectively Targets Resistant and Biofilm Gram-Negative Bacteria. *Biomaterials* **2023**, *294*, No. 122004.
(17) Limwongyut, J.; Liu, Y.; Chilambi, G. S.; Seviour, T.; Hinks, J.; Mu, Y.; Bazan, G. C. Interactions of a Paracyclophane-Based Conjugated Oligoelectrolyte with Biological Membranes. *RSC Adv.* **2018**, *8*, 39849−39853.
(18) Tian, J.; Zhang, J.; Yang, J.; Du, L.; Geng, H.; Cheng, Y. Conjugated Polymers Act Synergistically with Antibiotics to Combat Bacterial Drug Resistance. *ACS Appl. Mater. Interfaces* **2017**, *9*, 18512−18520.
(19) Chilambi, G. S.; Gao, I. H.; Yoon, K.; Park, S.; Kawakami, L. M.; Ravikumar, V.; Chan-Park, M. B.; Cho, N.-J.; Bazan, G. C.; Kline, K. A.; Rice, A.; Hinks, J. Membrane Adaptation Limitations in Enterococcus Faecalis Underlie Sensitivity and the Inability to Develop Significant Resistance to Conjugated Oligoelectrolytes. *RSC Adv.* **2018**, *8*, 10284−10293.
(20) Wang, Y.; Corbitt, T. S.; Jett, S. D.; Tang, Y.; Schanze, K. S.; Chi, E. Y.; Whitten, D. G. Direct Visualization of Bactericidal Action of Cationic Conjugated Polyelectrolytes and Oligomers. *Langmuir* **2012**, *28*, 65−70.
(21) Wang, B.; Wang, M.; Mikhailovsky, A.; Wang, S.; Bazan, G. C. A Membrane-Intercalating Conjugated Oligoelectrolyte with High-Efficiency Photodynamic Antimicrobial Activity. *Angew. Chem., Int. Ed.* **2017**, *56*, 5031−5034.
(22) Parthasarathy, A.; Pappas, H. C.; Hill, E. H.; Huang, Y.; Whitten, D. G.; Schanze, K. S. Conjugated Polyelectrolytes with Imidazolium Solubilizing Groups. Properties and Application to Photodynamic Inactivation of Bacteria. *ACS Appl. Mater. Interfaces* **2015**, *7*, 28027−28034.
(23) Xu, Q.; He, P.; Wang, J.; Chen, H.; Lv, F.; Liu, L.; Wang, S.; Yoon, J. Antimicrobial Activity of a Conjugated Polymer with Cationic Backbone. *Dyes Pigm.* **2019**, *160*, 519−523.
(24) Rabea, E. I.; Badawy, M. E. T.; Stevens, C. V.; Smagghe, G.; Steurbaut, W. Chitosan as Antimicrobial Agent: Applications and Mode of Action. *Biomacromolecules* **2003**, *4*, 1457−1465.
(25) Sahariah, P.; Másson, M. Antimicrobial Chitosan and Chitosan Derivatives : A Review of the Structure − Activity Relationship. *Biomacromolecules* **2017**, *18*, 3846−3868.
(26) Kumar, L.; Brice, J.; Toberer, L.; Klein-seetharaman, J.; Knauss, D.; Sarkar, S. K. Antimicrobial Biopolymer Formation from Sodium Alginate and Algae Extract Using Aminoglycosides. *PLoS One* **2019**, *14*, No. e0214411.
(27) Nemeş, N. S.; Ardean, C.; Davidescu, C. M.; Negrea, A.; Ciopec, M.; Duţeanu, N.; Negrea, P.; Paul, C.; Duda-Seiman, D.; Muntean, D. Antimicrobial Activity of Cellulose Based Materials. *Polymer* **2022**, *14*, 8−12.
(28) Zhang, Z.; Whitten, D. G.; Kell, A. Fluorescent Cellulose Wipe as a New and Sustainable Light-Activated Antibacterial and Antiviral Agent. *ACS Mater. Lett.* **2022**, *4*, 356−362.
(29) Wang, Y.; Li, Z.; Yang, D.; Qiu, X.; Xie, Y.; Zhang, X. Microwave-Mediated Fabrication of Silver Nanoparticles Incorporated Lignin-Based Composites with Enhanced Antibacterial Activity via Electrostatic Capture Effect. *J. Colloid Interface Sci.* **2021**, *583*, 80−88.
(30) Chee, P. L.; Owh, C.; Venkatesh, M.; Periayah, M. H.; Zhang, Z.; Michelle Yew, P. Y.; Ruan, H.; Lakshminarayanan, R.; Kai, D.; Loh, X. J. Cationic Lignin-Based Hyperbranched Polymers to Circumvent Drug Resistance in Pseudomonas Keratitis. *ACS Biomater. Sci. Eng.* **2021**, *7*, 4659−4668.
(31) Morena, A. G.; Bassegoda, A.; Natan, M.; Jacobi, G.; Banin, E.; Tzanov, T. Antibacterial Properties and Mechanisms of Action of Sonoenzymatically Synthesized Lignin-Based Nanoparticles. *ACS Appl. Mater. Interfaces* **2022**, *14*, 37270−37279.
(32) Yan, H.; Rengert, Z. D.; Thomas, A. W.; Rehermann, C.; Hinks, J.; Bazan, G. C. Influence of Molecular Structure on the Antimicrobial Function of Phenylenevinylene Conjugated Oligoelectrolytes. *Chem. Sci.* **2016**, *7*, 5714−5722.
(33) Heithoff, D. M.; Mahan, S. P.; Barnes, L.; Leyn, S. A.; George, C. X.; Zlamal, J. E.; Limwongyut, J.; Bazan, G. C.; Fried, J. C.; Fitzgibbons, L. N.; House, J. K.; Samuel, C. E.; Osterman, A. L.; Low, D. A.; Mahan, M. J. A Broad-Spectrum Synthetic Antibiotic That Does Not Evoke Bacterial Resistance. *eBioMedicine* **2023**, 1−13.
(34) Jacobson, K. H.; Gunsolus, I. L.; Kuech, T. R.; Troiano, J. M.; Melby, E. S.; Lohse, S. E.; Hu, D.; Chrisler, W. B.; Murphy, C. J.; Orr, G.; Geiger, F. M.; Haynes, C. L.; Pedersen, J. A. Lipopolysaccharide Density and Structure Govern the Extent and Distance of Nanoparticle Interaction with Actual and Model Bacterial Outer Membranes. *Environ. Sci. Technol.* **2015**, *49*, 10642−10650.
(35) Huang, Y. T.; Kumar, S. R.; Chan, H. C.; Jhan, Z. H.; Chen, D. W.; Lue, S. J. Efficacy of Antimicrobial Peptides (AMPs) against Escherichia Coli and Bacteria Morphology Change after AMP Exposure. *J. Taiwan Inst. Chem. Eng.* **2021**, *126*, 307−312.
(36) Seyfi, R.; Kahaki, F. A.; Ebrahimi, T.; Montazersaheb, S.; Eyvazi, S.; Babaeipour, V.; Tarhriz, V. Antimicrobial Peptides (AMPs): Roles, Functions and Mechanism of Action. *Int. J. Pept. Res. Ther.* **2020**, *26*, 1451−1463.
(37) Ebbensgaard, A.; Mordhorst, H.; Overgaard, M. T.; Nielsen, C. G.; Aarestrup, F. M.; Hansen, E. B. Comparative Evaluation of the Antimicrobial Activity of Different Antimicrobial Peptides against a Range of Pathogenic Bacteria. *PLoS One* **2015**, *10*, No. e0144611.
(38) Limwongyut, J.; Nie, C.; Moreland, A. S.; Bazan, G. C. Molecular Design of Antimicrobial Conjugated Oligoelectrolytes with Enhanced Selectivity toward Bacterial Cells. *Chem. Sci.* **2020**, *11*, 8138−8144.
(39) Zhang, C.; Wang, K.; Guo, X.; Tang, Y. A Cationic Conjugated Polymer with High 808 Nm NIR-Triggered Photothermal Conversion for Antibacterial Treatment. *J. Mater. Chem. C* **2022**, *10*, 2600−2607.
(40) Richter, A. P.; Brown, J. S.; Bharti, B.; Wang, A.; Gangwal, S.; Houck, K.; Cohen Hubal, E. A.; Paunov, V. N.; Stoyanov, S. D.; Velev, O. D. An Environmentally Benign Antimicrobial Nanoparticle

Based on a Silver-Infused Lignin Core. *Nat. Nanotechnol.* **2015**, *10*, 817−823.
(41) Islan, G. A.; Das, S.; Cacicedo, M. L.; Halder, A.; Mukherjee, A.; Cuestas, M. L.; Roy, P.; Castro, G. R.; Mukherjee, A. Silybin-Conjugated Gold Nanoparticles for Antimicrobial Chemotherapy against Gram-Negative Bacteria. *J. Drug Delivery Sci. Technol.* **2019**, *53*, No. 101181.
(42) Rocca, D. M.; Vanegas, J. P.; Fournier, K.; Becerra, M. C.; Scaiano, J. C.; Lanterna, A. E. Biocompatibility and Photo-Induced Antibacterial Activity of Lignin-Stabilized Noble Metal Nanoparticles. *RSC Adv.* **2018**, *8*, 40454−40463.
(43) Sinisi, V.; Pelagatti, P.; Carcelli, M.; Migliori, A.; Mantovani, L.; Righi, L.; Leonardi, G.; Pietarinen, S.; Hubsch, C.; Rogolino, D. A Green Approach to Copper-Containing Pesticides: Antimicrobial and Antifungal Activity of Brochantite Supported on Lignin for the Development of Biobased Plant Protection Products. *ACS Sustainable Chem. Eng.* **2019**, *7*, 3213−3221.
(44) da Silva Junior, A.; Teschke, O. Dynamics of the Antimicrobial Peptide PGLa Action on Escherichia Coli Monitored by Atomic Force Microscopy. *World J. Microbiol. Biotechnol.* **2005**, *21*, 1103−1110.
(45) Lam, N. H.; Ma, Z.; Ha, B. Y. Electrostatic Modification of the Lipopolysaccharide Layer: Competing Effects of Divalent Cations and Polycationic or Polyanionic Molecules. *Soft Matter* **2014**, *10*, 7528−7544.
(46) Shaw, J. E.; Epand, R. F.; Hsu, J. C. Y.; Mo, G. C. H.; Epand, R. M.; Yip, C. M. Cationic Peptide-Induced Remodelling of Model Membranes: Direct Visualization by in Situ Atomic Force Microscopy. *J. Struct. Biol.* **2008**, *162*, 121−138.
(47) Alves, E.; Santos, N.; Melo, T.; Maciel, E.; Dória, M. L.; Faustino, M. A. F.; Tomé, J. P. C.; Neves, M. G. P. M. S.; Cavaleiro, J. A. S.; Cunha, Â.; Helguero, L. A.; Domingues, P.; Almeida, A.; Domingues, M. R. M. Photodynamic Oxidation of Escherichia Coli Membrane Phospholipids: New Insights Based on Lipidomics. *Rapid Commun. Mass Spectrom.* **2013**, *27*, 2717−2728.
(48) Epand, R. M.; Epand, R. F. Lipid Domains in Bacterial Membranes and the Action of Antimicrobial Agents. *Biochim. Biophys. Acta, Biomembr.* **2009**, *1788*, 289−294.
(49) Alves, C. S.; Melo, M. N.; Franquelim, H. G.; Ferre, R.; Planas, M.; Feliu, L.; Bardají, E.; Kowalczyk, W.; Andreu, D.; Santos, N. C.; Fernandes, M. X.; Castanho, M. A. R. B. Escherichia Coli Cell Surface Perturbation and Disruption Induced by Antimicrobial Peptides BP100 and PepR. *J. Biol. Chem.* **2010**, *285*, 27536−27544.
(50) Wang, Y.; Jett, S. D.; Crum, J.; Schanze, K. S.; Chi, E. Y.; Whitten, D. G. Understanding the Dark and Light-Enhanced Bactericidal Action of Cationic Conjugated Polyelectrolytes and Oligomers. *Langmuir* **2013**, *29*, 781−792.
(51) Meincken, M.; Holroyd, D. L.; Rautenbach, M. Atomic Force Microscopy Study of the Effect of Antimicrobial Peptides on the Cell Envelope of Escherichia Coli. *Antimicrob. Agents Chemother.* **2005**, *49*, 4085−4092.
(52) Zhao, Y.; An, J.; Su, H.; Li, B.; Liang, D.; Huang, C. Antimicrobial Food Packaging Integrating Polysaccharide-Based Substrates with Green Antimicrobial Agents: A Sustainable Path. *Food Res. Int.* **2022**, *155*, No. 111096.
(53) Shu, H.; Zhang, W.; Yun, Y.; Chen, W.; Zhong, Q.; Hu, Y.; Chen, H.; Chen, W. Metabolomics Study on Revealing the Inhibition and Metabolic Dysregulation in Pseudomonas Fluorescens Induced by 3-Carene. *Food Chem.* **2020**, *329*, 1−11.
(54) Coronado, M. A.; de Moraes, F. R.; Stuqui, B.; Calmon, M. F.; Eberle, R. J.; Rahal, P.; Arni, R. K. The Secreted Metabolome of Hela Cells under Effect of Crotamine, a Cell-Penetrating Peptide from a Rattlesnake Using NMR-Based Metabolomics Analyses. *BioMed* **2022**, *2*, 238−254.
(55) Hussein, M.; Karas, J. A.; Schneider-Futschik, E. K.; Chen, F.; Swarbrick, J.; Paulin, O. K. A.; Hoyer, D.; Baker, M.; Zhu, Y.; Li, J.; Velkov, T. The Killing Mechanism of Teixobactin against Methicillin-Resistant Staphylococcus Aureus: An Untargeted Metabolomics Study. *mSystems* **2020**, *5*, 1−16.
(56) Polianciuc, S. I.; Gurzău, A. E.; Kiss, B.; Ştefan, M. G.; Loghin, F. Antibiotics in the Environment: Causes and Consequences. *Med. Pharm. Rep.* **2020**, *93*, 231−240.
(57) Garibo Ruiz, D.; Nefedova, E.; Shkil, N. N.; Shkil, N. A.; Vazquez-Gomez, R. L.; Pestryakov, A.; Bogdanchikova, N. Silver Nanoparticles Targeting the Drug Resistance Problem of Streptococcus Dysgalactiae: Susceptibility to Antibiotics and Efflux Effect. *Int. J. Mol. Sci.* **2022**, *23*, 6024.
(58) Lizundia, E.; Kundu, D. Advances in Natural Biopolymer-Based Electrolytes and Separators for Battery Applications. *Adv. Funct. Mater.* **2021**, *31*, 2005646.
(59) Aro, T.; Fatehi, P. Production and Application of Lignosulfonates and Sulfonated Lignin. *ChemSusChem* **2017**, *10*, 1861−1877.
(60) Xu, R.; Zhang, K.; Liu, P.; Han, H.; Zhao, S.; Kakade, A.; Khan, A.; Du, D.; Li, X. Lignin Depolymerization and Utilization by Bacteria. *Bioresour. Technol.* **2018**, *269*, 557−566.
(61) Ragauskas, A. J.; Beckham, G. T.; Biddy, M. J.; Chandra, R.; Chen, F.; Davis, M. F.; Davison, B. H.; Dixon, R. A.; Gilna, P.; Keller, M.; Langan, P.; Naskar, A. K.; Saddler, J. N.; Tschaplinski, T. J.; Tuskan, G. A.; Wyman, C. E. Lignin Valorization: Improving Lignin Processing in the Biorefinery. *Science* **2014**, *344*, 1246843.
(62) Bajwa, D. S.; Pourhashem, G.; Ullah, A. H.; Bajwa, S. G. A Concise Review of Current Lignin Production, Applications, Products and Their Environment Impact. *Ind. Crops Prod.* **2019**, *139*, No. 111526.
(63) Xie, S.; Ragauskas, A. J.; Yuan, J. S. Lignin Conversion: Opportunities and Challenges for the Integrated Biorefinery. *Ind. Biotechnol.* **2016**, *12*, 161−167.
(64) Farzin, S.; Johnson, T. J.; Chatterjee, S.; Zamani, E.; Dishari, S. K. Ionomers From Kraft Lignin for Renewable Energy Applications. *Front. Chem.* **2020**, *8*, 690.
(65) Wu, X.; Jiang, J.; Wang, C.; Liu, J.; Pu, Y.; Ragauskas, A.; Li, S.; Yang, B. Lignin-Derived Electrochemical Energy Materials and Systems. *Bioprod. Biorefin.* **2020**, *14*, 650−672.
(66) Farzin, S.; Acurio Cerda, K.; Obewhere, O. A.; Dishari, S. K. Lignin-Based Materials for Energy Conversion and Storage Devices. In *Sustainability Engineering Challenges, Technologies, and Applications*; Tan, E. C. D., Ed.; Taylor & Francis Group: 2023; pp. 1−60.
(67) Wang, S.; Bai, J.; Innocent, M. T.; Wang, Q.; Xiang, H.; Tang, J.; Zhu, M. Lignin-Based Carbon Fibers: Formation, Modification and Potential Applications. *Green Energy Environ.* **2022**, *7*, 578−605.
(68) Mahajan, J. S.; O'Dea, R. M.; Norris, J. B.; Korley, S. T. J.; Epps, T. H. Aromatics from Lignocellulosic Biomass: A Platform for High-Performance Thermosets. *ACS Sustainable Chem. Eng.* **2020**, *8*, 15072−15096.
(69) Sipponen, M. H.; Lange, H.; Crestini, C.; Henn, A.; Österberg, M. Lignin for Nano- and Microscaled Carrier Systems: Applications, Trends, and Challenges. *ChemSusChem* **2019**, *12*, 2039−2054.
(70) Matos, M.; Claro, F. C.; Lima, T. A. M.; Avelino, F.; Hansel, F. A.; Maciel, G. M.; Lomonaco, D.; Magalhães, W. L. E. Acetone:Water Fractionation of Pyrolytic Lignin Improves Its Antioxidant and Antibacterial Activity. *J. Anal. Appl. Pyrolysis* **2021**, *156*, No. 105175.
(71) Lourençon, T. V.; de Lima, G. G.; Ribeiro, C. S. P.; Hansel, F. A.; Maciel, G. M.; da Silva, K.; Winnischofer, S. M. B.; de Muniz, G. I. B.; Magalhães, W. L. E. Antioxidant, Antibacterial and Antitumoural Activities of Kraft Lignin from Hardwood Fractionated by Acid Precipitation. *Int. J. Biol. Macromol.* **2021**, *166*, 1535−1542.
(72) Ran, F.; Li, C.; Hao, Z.; Zhang, X.; Dai, L.; Si, C.; Shen, Z.; Qiu, Z.; Wang, J. Combined Bactericidal Process of Lignin and Silver in a Hybrid Nanoparticle on *E. coli*. *Adv. Comp. Hybrid Mater.* **2022**, *5*, 1841−1851.
(73) Klapiszewski, Ł.; Rzemieniecki, T.; Krawczyk, M.; Malina, D.; Norman, M.; Zdarta, J.; Majchrzak, I.; Dobrowolska, A.; Czaczyk, K.; Jesionowski, T. Kraft Lignin/Silica-AgNPs as a Functional Material with Antibacterial Activity. *Colloids Surf., B* **2015**, *134*, 220−228.
(74) Li, Y.; Yang, D.; Li, P.; Li, Z. Lignin as a Multi-Functional Agent for the Synthesis of Ag Nanoparticles and Its Application in Antibacterial Coatings. *J. Mater. Res. Technol.* **2022**, *17*, 3211−3220.

(75) Yang, W.; Fortunati, E.; Gao, D.; Balestra, G. M.; Giovanale, G.; He, X.; Torre, L.; Kenny, J. M.; Puglia, D. Valorization of Acid Isolated High Yield Lignin Nanoparticles as Innovative Antioxidant/Antimicrobial Organic Materials. *ACS Sustainable Chem. Eng.* **2018**, *6*, 3502−3514.
(76) Sirviö, J. A.; Ismail, M. Y.; Zhang, K.; Tejesvi, M. V.; Ämmälä, A. Transparent Lignin-Containing Wood Nanofiber Films with UV-Blocking, Oxygen Barrier, and Anti-Microbial Properties. *J. Mater. Chem. A* **2020**, *8*, 7935−7946.
(77) Ma, Y.; Dai, J.; Wu, L.; Fang, G.; Guo, Z. Enhanced Anti-Ultraviolet, Anti-Fouling and Anti-Bacterial Polyelectrolyte Membrane of Polystyrene Grafted with Trimethyl Quaternary Ammonium Salt Modified Lignin. *Polymer* **2017**, *114*, 113−121.
(78) An, L.; Heo, J. W.; Chen, J.; Kim, Y. S. Water-Soluble Lignin Quaternary Ammonium Salt for Electrospun Morphology-Controllable Antibacterial Polyvinyl Alcohol/ Lignin Quaternary Ammonium Salt Nanofibers. *J. Cleaner Prod.* **2022**, *368*, No. 133219.
(79) Fu, C.; Donovan, W. P.; Shikapwashya-Hasser, O.; Ye, X.; Cole, R. H. Hot Fusion: An Efficient Method to Clone Multiple DNA Fragments as Well as Inverted Repeats without Ligase. *PLoS One* **2014**, *9*, No. e115318.
(80) Kong, F.; Parhiala, K.; Wang, S.; Fatehi, P. Preparation of Cationic Softwood Kraft Lignin and Its Application in Dye Removal. *Eur. Polym. J.* **2015**, *67*, 335−345.
(81) Rivière, G. N.; Korpi, A.; Sipponen, M. H.; Zou, T.; Kostiainen, M. A.; Österberg, M. Agglomeration of Viruses by Cationic Lignin Particles for Facilitated Water Purification. *ACS Sustainable Chem. Eng.* **2020**, *8*, 4167−4177.
(82) Wahlström, R.; Kalliola, A.; Heikkinen, J.; Kyllönen, H.; Tamminen, T. Lignin Cationization with Glycidyltrimethylammonium Chloride Aiming at Water Purification Applications. *Ind. Crops Prod.* **2017**, *104*, 188−194.
(83) Argyropoulos, D. S.; Pajer, N.; Crestini, C. Quantitative 31P NMR Analysis of Lignins and Tannins. *J. Visualized Exp.* **2021**, *2021*, No. e62696.
(84) Zhao, W.; Xiao, L. P.; Song, G.; Sun, R. C.; He, L.; Singh, S.; Simmons, B. A.; Cheng, G. From Lignin Subunits to Aggregates: Insights into Lignin Solubilization. *Green Chem.* **2017**, *19*, 3272−3281.
(85) Zhang, P.-Y.; Xu, P.-P.; Xia, Z.-J.; Wang, J.; Xiong, J.; Li, Y.-Z. Combined Treatment with the Antibiotics Kanamycin and Streptomycin Promotes the Conjugation of Escherichia Coli. *FEMS Microbiol. Lett.* **2013**, *348*, 149−156.
(86) *Molecular Probes Inc. LIVE/DEAD® BacLight™ Bacterial Viability and Counting Kit*. 2004, pp. 1−5.
(87) Liu, L.; Bhatia, R.; Webster, T. Atomic Layer Deposition of Nano-TiO2 Thin Films with Enhanced Biocompatibility and Antimicrobial Activity for Orthopedic Implants. *Int. J. Nanomed.* **2017**, *Volume 12*, 8711−8723.
(88) Yao, J.; Zhang, M.; Han, F.; Liu, Z.; Han, Y.; Li, Q.; Zhou, W. Thermophilic Adsorption of Pb2+ onto Bacterium from Deep-Sea Hydrothermal Vent. *J. Environ. Chem. Eng.* **2022**, *10*, No. 107364.
(89) Borthakur, P.; Hussain, N.; Darabdhara, G.; Boruah, P. K.; Sharma, B.; Borthakur, P.; Yadav, A.; Das, M. R. Adhesion of Gram-Negative Bacteria onto α-Al2O3 Nanoparticles: A Study of Surface Behaviour and Interaction Mechanism. *J. Environ. Chem. Eng.* **2018**, *6*, 3933−3941.
(90) Ajeng, A. A.; Abdullah, R.; Ling, T. C.; Ismail, S. Adhesion of Bacillus Salmalaya and Bacillus Amyloliquefaciens on Oil Palm Kernel Shell Biochar: A Physicochemical Approach. *J. Environ. Chem. Eng.* **2022**, *10*, No. 107115.
(91) Atoufi, Z.; Cinar Ciftci, G.; Reid, M. S.; Larsson, P. A.; Wågberg, L. Green Ambient-Dried Aerogels with a Facile PH-Tunable Surface Charge for Adsorption of Cationic and Anionic Contaminants with High Selectivity. *Biomacromolecules* **2022**, *23*, 4934−4947.
(92) Wen, T.; Wang, J.; Yu, S.; Chen, Z.; Hayat, T.; Wang, X. Magnetic Porous Carbonaceous Material Produced from Tea Waste for Efficient Removal of As(V), Cr(VI), Humic Acid, and Dyes. *ACS Sustainable Chem. Eng.* **2017**, *5*, 4371−4380.
(93) Tran-ly, A. N.; De France, K. J.; Rupper, P.; Schwarze, F. W. M. R.; Reyes, C.; Nyström, G.; Siqueira, G.; Ribera, J. Melanized-Cationic Cellulose Nanofiber Foams for Bioinspired Removal of Cationic Dyes. *Biomacromolecules* **2021**, *22*, 4681−4690.
(94) Alshehri, S. M.; Naushad, M.; Ahamad, T.; Alothman, Z. A.; Aldalbahi, A. Synthesis, Characterization of Curcumin Based Ecofriendly Antimicrobial Bio-Adsorbent for the Removal of Phenol from Aqueous Medium. *Chem. Eng. J.* **2014**, *254*, 181−189.
(95) Othman, A.; Dumitrescu, E.; Andreescu, D.; Andreescu, S. Nanoporous Sorbents for the Removal and Recovery of Phosphorus from Eutrophic Waters: Sustainability Challenges and Solutions. *ACS Sustainable Chem. Eng.* **2018**, *6*, 12542−12561.
(96) Ramalingam, B.; Parandhaman, T.; Choudhary, P.; Das, S. K. Biomaterial Functionalized Graphene-Magnetite Nanocomposite: A Novel Approach for Simultaneous Removal of Anionic Dyes and Heavy-Metal Ions. *ACS Sustainable Chem. Eng.* **2018**, *6*, 6328−6341.
(97) Cai, Z.; Wang, Y.; Zhang, Y.; Tian, H. Effects of Surfactant on Bacillus Mucilaginosus Adsorption Characteristics during Vanadium Bioleaching Process. *J. Environ. Chem. Eng.* **2022**, *10*, 1−8.
(98) Asfaram, A.; Ghaedi, M.; Dashtian, K.; Ghezelbash, G. R. Preparation and Characterization of Mn0.4Zn0.6Fe2O4 Nanoparticles Supported on Dead Cells of Yarrowia Lipolytica as a Novel and Efficient Adsorbent/Biosorbent Composite for the Removal of Azo Food Dyes: Central Composite Design Optimization Study. *ACS Sustainable Chem. Eng.* **2018**, *6*, 4549−4563.
(99) Feng, X.; Jin, S.; Wang, M.; Pang, Q.; Liu, C.; Liu, R.; Wang, Y.; Yang, H.; Liu, F.; Liu, Y. The Critical Role of Tryptophan in the Antimicrobial Activity and Cell Toxicity of the Duck Antimicrobial Peptide DCATH. *Front. Microbiol.* **2020**, *11*, 1146.
(100) Kim, J.; Jacob, B.; Jang, M.; Kwak, C.; Lee, Y.; Son, K.; Lee, S.; Jung, I. D.; Jeong, M. S.; Kwon, S. H.; Kim, Y. Development of a Novel Short 12-Meric Papiliocin-Derived Peptide That Is Effective against Gram-Negative Sepsis. *Sci. Rep.* **2019**, *9*, 3817.
(101) Chen, J.; Shan, J.; Xu, Y.; Su, P.; Tong, L.; Yuwen, L.; Weng, L.; Bao, B.; Wang, L. Polyhedral Oligomeric Silsesquioxane (POSS)-Based Cationic Conjugated Oligoelectrolyte / Porphyrin for E Ffi Cient Energy Transfer and Multiampli Fi Ed Antimicrobial Activity. *ACS Appl. Mater. Interfaces* **2018**, *10*, 34455−34463.
(102) Wei, Y.; Cheng, F.; Zheng, H. Synthesis and Flocculating Properties of Cationic Starch Derivatives. *Carbohydr. Polym.* **2008**, *74*, 673−679.
(103) Liu, Z.; Ni, Y.; Fatehi, P.; Saeed, A. Isolation and Cationization of Hemicelluloses from Pre-Hydrolysis Liquor of Kraft-Based Dissolving Pulp Production Process. *Biomass Bioenergy* **2011**, *35*, 1789−1796.
(104) Cho, J.; Grant, J.; Piquette-miller, M.; Allen, C. Synthesis and Physicochemical and Dynamic Mechanical Properties of a Water-Soluble Chitosan Derivative as a Biomaterial. *Biomacromolecules* **2006**, *7*, 2845−2855.
(105) Phuangkaew, T.; Booranabunyat, N.; Kiatkamjornwong, S.; Thanyasrisung, P.; Hoven, V. P. Amphiphilic Quaternized Chitosan : Synthesis , Characterization , and Anti-Cariogenic Biofilm Property. *Carbohydr. Polym.* **2022**, *277*, No. 118882.
(106) Pinto, P. I. F.; Magina, S.; Budjav, E.; Pinto, P. C. R.; Liebner, F.; Evtuguin, D. Cationization of Eucalyptus Kraft LignoBoost Lignin: Preparation, Properties, and Potential Applications. *Ind. Eng. Chem. Res.* **2022**, *61*, 3503−3515.
(107) Chen, D.; Hickner, M. A. Degradation of Imidazolium- and Quaternary Ammonium-Functionalized Poly(Fluorenyl Ether Ketone Sulfone) Anion Exchange Membranes. *ACS Appl. Mater. Interfaces* **2012**, *4*, 5775−5781.
(108) Matica, M. A.; Aachmann, F. L.; Tøndervik, A.; Sletta, H.; Ostafe, V. Chitosan as a Wound Dressing Starting Material: Antimicrobial Properties and Mode of Action. *Int. J. Mol. Sci.* **2019**, *20*, 5889.

(109) Morena, A. G.; Bassegoda, A.; Hoyo, J.; Tzanov, T. Hybrid Tellurium-Lignin Nanoparticles with Enhanced Antibacterial Properties. *ACS Appl. Mater. Interfaces* **2021**, *13*, 14885−14893.
(110) Avalos Vizcarra, I.; Emge, P.; Miermeister, P.; Chabria, M.; Konradi, R.; Vogel, V.; Möller, J. Fluorescence-Based in Situ Assay to Probe the Viability and Growth Kinetics of Surface-Adhering and Suspended Recombinant Bacteria. *Biointerphases* **2013**, *8*, 22.
(111) Catania, C.; Thomas, A. W.; Bazan, G. C. Tuning Cell Surface Charge in E. Coli with Conjugated Oligoelectrolytes. *Chem. Sci.* **2016**, *7*, 2023−2029.
(112) Xu, W. Z.; Yang, L.; Charpentier, P. A. Preparation of Antibacterial Softwood via Chemical Attachment of Quaternary Ammonium Compounds Using Supercritical CO2. *ACS Sustainable Chem. Eng.* **2016**, *4*, 1551−1561.
(113) Das, B.; Dash, S. K.; Mandal, D.; Ghosh, T.; Chattopadhyay, S.; Tripathy, S.; Das, S.; Dey, S. K.; Das, D.; Roy, S. Green Synthesized Silver Nanoparticles Destroy Multidrug Resistant Bacteria via Reactive Oxygen Species Mediated Membrane Damage. *Arabian J. Chem.* **2017**, *10*, 862−876.
(114) Arshad, H.; Sadaf, S.; Hassan, U. De-Novo Fabrication of Sunlight Irradiated Silver Nanoparticles and Their Efficacy against E. Coli and S. Epidermidis. *Sci. Rep.* **2022**, *12*, 1−10.
(115) Wang, Y.; Zhou, Z.; Zhu, J.; Tang, Y.; Canady, T. D.; Chi, E. Y.; Schanze, K. S.; Whitten, D. G. Dark Antimicrobial Mechanisms of Cationic Phenylene Ethynylene Polymers and Oligomers against Escherichia Coli. *Polymer* **2011**, *3*, 1199−1214.
(116) Choi, H.; Chakraborty, S.; Liu, R.; Gellman, S. H.; Weisshaar, J. C. Medium Effects on Minimum Inhibitory Concentrations of Nylon-3 Polymers against *E. coli*. *PLoS One* **2014**, *9*, No. e104500.
(117) Xu, X.; Ou, Z. M.; Wu, C. D. Growth Media Affect Assessment of Antimicrobial Activity of Plant-Derived Polyphenols. *BioMed Res. Int.* **2018**, *2018*, 1−7.
(118) Franz, B.; Balkundi, S. S.; Dahl, C.; Lvov, Y. M.; Prange, A. Layer-by-Layer Nano-Encapsulation of Microbes: Controlled Cell Surface Modification and Investigation of Substrate Uptake in Bacteria. *Macromol. Biosci.* **2010**, *10*, 164−172.
(119) Balkundi, S. S.; Veerabadran, N. G.; Eby, D. M.; Johnson, G. R.; Lvov, Y. M. Encapsulation of Bacterial Spores in Nanoorganized Polyelectrolyte Shells. *Langmuir* **2009**, *25*, 14011−14016.
(120) Zhu, C.; Yang, Q.; Lv, F.; Liu, L.; Wang, S. Conjugated Polymer-Coated Bacteria for Multimodal Intracellular and Extracellular Anticancer Activity. *Adv. Mater.* **2013**, *25*, 1203−1208.
(121) Ren, X.; Hao, J.; Guo, L.; Sathishkumar, G.; Xu, L. Quaternary Ammonium Functionalized Cationic Polythiophene for the Detection and Imaging of Gram-Positive Bacteria. *Polym. Bull.* **2022**, *79*, 2747−2761.
(122) Rittig, M. G.; Kaufmann, A.; Robins, A.; Shaw, B.; Sprenger, H.; Gemsa, D.; Foulongne, V.; Rouot, B.; Dornand, J. Smooth and Rough Lipopolysaccharide Phenotypes of Brucella Induce Different Intracellular Trafficking and Cytokine/Chemokine Release in Human Monocytes. *J. Leukocyte Biol.* **2003**, *74*, 1045−1055.
(123) Li, A.; Lee, P. Y.; Ho, B.; Ding, J. L.; Lim, C. T. Atomic Force Microscopy Study of the Antimicrobial Action of Sushi Peptides on Gram Negative Bacteria. *Biochim. Biophys. Acta, Biomembr.* **2007**, *1768*, 411−418.
(124) Spiekermann, P.; Rehm, B. H. A.; Kalscheuer, R.; Baumeister, D.; Steinbüchel, A. A Sensitive, Viable-Colony Staining Method Using Nile Red for Direct Screening of Bacteria That Accumulate Polyhydroxyalkanoic Acids and Other Lipid Storage Compounds. *Arch. Microbiol.* **1999**, *171*, 73−80.
(125) Greenspan, P.; Mayer, E. P.; Fowler, S. D. Nile Red: A Selective Fluorescent Stain for Intracellular Lipid Droplets. *J. Cell Biol.* **1985**, *100*, 965−973.
(126) Lázaro, B.; Villa, J. A.; Santín, O.; Cabezas, M.; Milagre, C. D. F.; De La Cruz, F.; Moncalián, G. Heterologous Expression of a Thermophilic Diacylglycerol Acyltransferase Triggers Triglyceride Accumulation in Escherichia Coli. *PLoS One* **2017**, *12*, No. e0176520.
(127) Chng, S. S.; Ruiz, N.; Chimalakonda, G.; Silhavy, T. J.; Kahne, D. Characterization of the Two-Protein Complex in Escherichia Coli Responsible for Lipopolysaccharide Assembly at the Outer Membrane. *Proc. Natl. Acad. Sci.* **2010**, *107*, 5363−5368.
(128) Martorana, A. M.; Motta, S.; Di Silvestre, D.; Falchi, F.; Dehò, G.; Mauri, P.; Sperandeo, P.; Polissi, A. Dissecting Escherichia Coli Outer Membrane Biogenesis Using Differential Proteomics. *PLoS One* **2014**, *9*, No. e100941.
(129) Nikaido, H.; Vaara, M. Molecular Basis of Bacterial Outer Membrane Permeability. *Microbiol. Rev.* **1985**, *49*, 1−32.
(130) Kotra, L. P.; Golemi, D.; Amro, N. A.; Liu, G.-Y.; Mobashery, S. Dynamics of the Lipopolysaccharide Assembly on the Surface of Escherichia Coli. *J. Am. Chem. Soc.* **2016**, *121*, 8707−8711.
(131) Clifton, L. A.; Skoda, M. W.; Daulton, E. L.; Hughes, A. V.; Le Brun, A. P.; Lakey, J. H.; Holt, S. A. Asymmetric Phospholipid: Lipopolysaccharide Bilayers; a Gram-Negative Bacterial Outer Membrane Mimic. *J. R. Soc., Interface* **2013**, *10*, 20130810.
(132) Silhavy, T. J.; Kahne, D.; Walker, S. The Bacterial Cell Envelope. *Cold Spring Harbor Perspect. Biol.* **2010**, *2*, 1−16.
(133) Malanovic, N.; Lohner, K. Gram-Positive Bacterial Cell Envelopes: The Impact on the Activity of Antimicrobial Peptides. *Biochim. Biophys. Acta, Biomembr.* **2016**, *1858*, 936−946.
(134) Goyal, R. K.; Mattoo, A. K. Plant Antimicrobial Peptides. In *Host Defense Peptides and Their Potential as Therapeutic Agents*; Springer: 2016; pp. 111−136, DOI: 10.1007/978-3-319-32949-9_5.
(135) Shai, Y. Mechanism of the Binding, Insertion and Destabilization of Phospholipid Bilayer Membranes by Alpha-Helical Antimicrobial and Cell Non-Selective Membrane-Lytic Peptides. *Biochim. Biophys. Acta, Biomembr.* **1999**, *1462*, 55−70.
(136) Galbadage, T.; Liu, D.; Alemany, L. B.; Pal, R.; Tour, J. M.; Gunasekera, R. S.; Cirillo, J. D. Molecular Nanomachines Disrupt Bacterial Cell Wall, Increasing Sensitivity of Extensively Drug Resistant Klebsiella Pneumoniae to Meropenem. *ACS Nano* **2019**, *13*, 14377−14387.
(137) Sun, C.; Gu, L.; Hussain, M. A.; Chen, L.; Lin, L.; Wang, H.; Pang, S.; Jiang, C.; Jiang, Z.; Hou, J. Characterization of the Bioactivity and Mechanism of Bactenecin Derivatives Against Food-Pathogens. *Front. Microbiol.* **2019**, *10*, 2593.
(138) Arias, M.; Mcdonald, L. J.; Haney, E. F.; Nazmi, K.; Bolscher, J. G. M.; Vogel, H. J. Bovine and Human Lactoferricin Peptides: Chimeras and New Cyclic Analogs. *BioMetals* **2014**, *27*, 935−948.
(139) Nishino, M.; Matsuzaki, I.; Musangile, F. Y.; Takahashi, Y.; Iwahashi, Y.; Warigaya, K.; Kinoshita, Y.; Kojima, F.; Murata, S. Measurement and Visualization of Cell Membrane Surface Charge in Fixed Cultured Cells Related with Cell Morphology. *PLoS One* **2020**, *15*, No. e0236373.